Proteomic phenotyping of stimulated Müller cells uncovers profound pro-inflammatory signaling and antigen-presenting capacity

Adrian Schmalen[1,2], Lea Lorenz[2], Antje Grosche[3], Diana Pauly[4,5], Cornelia A. Deeg[2], Stefanie M. Hauck[1*]

[1]Research Unit Protein Science and Metabolomics and Proteomics Core, Helmholtz Center Munich, German Research Center for Environmental Health, D-85764 Neuherberg, Germany

[2]Chair of Physiology, Department of Veterinary Sciences, LMU Munich, D-82152 Martinsried, Germany

[3]Department of Physiological Genomics, Biomedical Center, LMU Munich, D-82152 Martinsried, Germany

[4]Experimental Ophthalmology, Philipps-University Marburg, D-35043 Marburg, Germany

[5]Department of Ophthalmology, University Hospital Regensburg, D-93053 Regensburg, Germany

*** Correspondence:**
Corresponding Author
hauck@helmholtz-muenchen.de

Keywords: Müller cells, atypical antigen-presenting cell, immune response, diabetic retinopathy, oxidative phosphorylation, complement system, cytokines, retina.

Abstract

Müller cells are the main macroglial cells of the retina exerting a wealth of functions to maintain retinal homoeostasis. Upon pathological changes in the retina, they become gliotic with both protective and detrimental consequences. Accumulating data also provide evidence for a pivotal role of Müller cells in the pathogenesis of diabetic retinopathy (DR). While microglial cells, the resident immune cells of the retina are considered as main players in inflammatory processes associated with DR, the implication of activated Müller cells in chronic retinal inflammation remains to be elucidated. In order to assess the signaling capacity of Müller cells and their role in retinal inflammation, we performed in-depth proteomic analysis of Müller cell proteomes and secretomes after stimulation with INFγ, TNFα, IL-4, IL-6, IL-10, VEGF, TGFβ1, TGFβ2 and TGFβ3. We used both, primary porcine Müller cells and the human Müller cell line MIO-M1 for our hypothesis generating approach. Our results point towards an intense signaling capacity of Müller cells, which reacted in a highly discriminating manner upon treatment with different cytokines. Stimulation of Müller cells resulted in a primarily pro-inflammatory phenotype with secretion of cytokines and components of the complement system. Furthermore, we observed evidence for mitochondrial dysfunction, implying oxidative stress after treatment with the various cytokines. Finally, both MIO-M1 cells and primary porcine Müller cells showed several characteristics of atypical antigen-presenting cells, as they are capable of inducing MHC class I and MHC class II with co-stimulatory molecules. In line with this, they express proteins associated with formation and maturation of phagosomes. Thus, our findings underline the importance of Müller cell signaling in the inflamed retina, indicating an active role in chronic retinal inflammation underlying the pathogenesis of diabetic retinopathy.

1 Introduction

Neurodegenerative diseases of the retina are characterized by progressive photoreceptor damage eventually resulting in vision loss (1). Accumulating evidence over the last years led to the recognition of chronic inflammation as an important part of the pathogenesis underlying this heterogeneous group of retinal diseases (2-4). While the loss of photoreceptors in inherited retinal diseases such as retinitis pigmentosa originates in various genetic mutations (5), the driving force that leads to retinal degeneration and blindness in diabetic retinopathy (DR) is a disturbed metabolism with hyperglycemia and dyslipidemia, resulting in microvascular damage (6). DR is among the most frequent causes of blindness worldwide with a rising prevalence (7). Chronic hyperglycemia in diabetes patients induces the activation of leukocytes in the periphery (8) as well as micro- and macroglial cells in the retina (9-11). This results in the release of pro-inflammatory cytokines and eventually leads to photoreceptor cell death (12, 13). Microglial cells, the resident immune cells of the retina, are acknowledged as the main drivers of retinal immune responses (14). However, growing evidence suggests that the interaction of micro- and macroglial cells essentially shapes retinal inflammation and photoreceptor degeneration (15, 16).

Retinal Müller glial cells constitute the primary macroglial cells of the retina (17). They span the entire width of the retina and are in close contact with the vitreous, the retinal blood-vessels and with all retinal neurons (18). While they maintain retinal homeostasis during steady-state conditions, activation of Müller cells under pathological conditions results in gliosis, a cellular attempt to restore insulted tissue, with both protective and detrimental effects (19). It is known that Müller cells are an important source of neurotrophic factors but also of pro-inflammatory and angiogenetic cytokines (20-23). They play an important role in DR pathogenesis (24, 25) and it was also suggested that they are involved in retinal immune responses (26-30). However, the impact of their protective or detrimental effects on retinal inflammation in DR and other neurodegenerative retinal diseases remains elusive so far. Thus, we performed an in-depth-analysis of the Müller cell proteome and secretome after stimulation with various pro- and anti-inflammatory cytokines as well as growth factors. For our analysis, we used cells of the human Müller glia cell-line MIO-M1 as well as primary porcine retinal Müller Glia (pRMG), as porcine eyes resemble human eyes regarding their anatomy (31). Furthermore, the pig is established as a useful model for research in diabetic retinopathy (32, 33). Comparative quantitative proteomic analysis allows to elucidate key proteins or pathways involved in disease pathogenesis. In addition, this approach enables the discovery of new biomarkers and has therefore proven as a valuable tool for deciphering pathophysiological key mechanisms (34, 35). Our hypothesis-generating study yielded comprehensive data on the capacity of Müller cells to react in a very differentiated manner to varying stimulants. In addition to the secretion of pro-inflammatory cytokines, we observed expression of MHC class I and II molecules and proteins that are associated with the processing of antigens. We therefore propose that Müller cells are critical modulators of the retinal immune response and might exert an antigen-presenting function. Thus, attention should be paid to their implication in chronic inflammation underlying degenerative retinal diseases.

2 Materials and methods

2.1 Cell preparation and culture

Cells were maintained in Dulbecco's modified eagle medium (DMEM) containing 10% (*v*/*v*) inactivated fetal calf serum (FCS), 100 U/mL penicillin and 100 µg/mL streptomycin unless

This is a provisional file, not the final typeset article

otherwise stated. Cell culture media and reagents were purchased from Gibco (Life Technologies GmbH, Darmstadt, Germany).

Ten porcine eyes from healthy pigs were kindly provided from a local abattoir. The use of porcine material from the abattoir was approved for purposes of scientific research by the appropriate board of the veterinary inspection office, Munich, Germany (registration number DE 09 162 0008-21). No experimental animals were involved in this study. Within 2h after enucleation, eyes were processed under a laminar flow hood under sterile conditions as previously described (30, 36). In short, periocular tissue was removed and the eyeballs were rinsed in 80% ethanol followed by washing with cold PBS. Afterwards, eyeballs were stored in DMEM until further processing. The eyeballs were opened circumferentially parallel to the limbus corneae, and anterior parts of the eyes were discarded. The retina was detached from the posterior eyeballs and transferred into a petri dish containing DMEM. After removal of vitreous and pigment epithelium residues, major blood-vessels were excised and the remaining retinal tissue was cut into very small fragments using micro-scissors. Resulting fragments were washed in Ringer's solution followed by enzymatic digestion at 37 °C with papain previously activated by incubation with 1.1 µM EDTA, 0.067 µM mercaptoethanol and 5.5 µM cysteine-HCl. Enzymatic digestion was stopped after 12 min by adding serum-containing DMEM, followed by addition of Desoxyribonuclease I (Sigma-Aldrich Chemie GmbH, Taufkirchen, Germany) and trituration. After sedimentation of the cells, the supernatant was carefully removed using Pasteur pipettes. The remaining pellets were resuspended in DMEM, pooled and seeded into 6-well plates (Sarstedt, Nümbrecht, Germany). The following day, thorough panning of the plates and removal of the supernatant were performed in order to eliminate non-attached cells, yielding pure Müller cell cultures as previously described (37, 38). Cells were cultured at 37 °C and 5% CO_2 with regular exchange of medium and repeated microscopic control of cell density and purity according to previous reports (37, 39).

The human Müller cell line Moorfields/Institute of Ophthalmology-Müller 1 (MIO-M1; RRID:CVCL_0433) was a kind gift of G. A. Limb (39). They were tested negative for mycoplasma contamination. Two days before treatment, 1×10^5 MIO-M1 cells per well were seeded in 6-well plates and incubated at 37 °C and 5% CO_2 until further processing.

2.2 Cell stimulation

The human cytokines Interleukin 10 (IL-10), Transforming Growth Factor beta-1 (TGFβ1), Transforming Growth Factor beta-2 (TGFβ2), Transforming Growth Factor beta-3 (TGFβ3), and Tumor Necrosis Factor Alpha (TNFα) were purchased from Sigma-Aldrich, Interleukin 4 (IL-4) and Interferon Gamma (IFNy) from R&D Systems/Bio-Techne (R&D Systems/Bio-Techne, Wiesbaden-Nordenstadt, Germany), and Interleukin 6 (IL-6) and Vascular Endothelial Growth $Factor_{165}$ (VEGF) from PeproTech (PeproTech, Winterhude, Germany). Porcine TGFβ3 was purchased from Biozol (Biozol, Eching, Germany), whereas porcine TGFβ1, TGFβ2, IL-4, IL-6, IL-10, IFNy and TNFα were from R&D System/Bio-Techne. Since there was no porcine VEGF available, the above mentioned human VEGF was also used for stimulation of pRMG.

To diminish the influence of cytokines present in FCS, both confluent pRMG and MIO-M1 cells were rinsed two times with prewarmed serum-free medium, followed by starvation for 1 h at 37 °C and 5% CO_2 with serum-deprived medium. Afterwards, cells were treated over night with IFNy, IL-4, IL-6, IL-10, TGFβ1, TGFβ2, TGFβ3, TNFα or $VEGF_{165}$, respectively, in a randomized plate design at a concentration of 5 ng/mL in medium without FCS. Untreated cells cultured in serum-free medium served as a control.

125 **2.3 Sample collection and proteolysis**

126 Supernatants were collected 24 h after treatment, passed through medium equilibrated 0.2 µm
127 Millex-GP filter units (Merck Chemicals GmbH, Darmstadt, Germany), and transferred into 2 mL
128 Lo-Bind tubes (Eppendorf AG, Hamburg, Germany). Afterwards, cells were washed once with
129 DPBS. 200 µL RIPA buffer containing Roche cOmplete Mini Protease Inhibitor Cocktail (Merck
130 Chemicals GmbH) was applied directly into each well and cells were detached with a cell scraper.
131 Lysates were transferred into freshly prepared 1.5 mL Lo-Bind tubes (Eppendorf AG). Protein
132 concentration of the lysates was determined by Pierce BCA assay (Thermo Fisher Scientific). Ten µg
133 protein per lysate or 400 µL supernatant per sample were digested with Lys-C and trypsin using a
134 modified FASP procedure as described elsewhere (40, 41).

135 **2.4 LC-MS/MS and quantitative analysis**

136 LC-MSMS analysis was performed on a QExactive HF mass spectrometer (Thermo Fisher Scientific)
137 online coupled to a UItimate 3000 RSLC nano-HPLC (Dionex, Sunnyvale, USA). Samples were
138 automatically injected and loaded onto a C18 trap column for 5 min. Afterwards, samples were eluted
139 and separated on a C18 analytical column (Acquity UPLC M-Class HSS T3 Column, 1.8 µm, 75 µm
140 × 250 mm; Waters, Milford, USA). Samples were separated by a 95 min non-linear acetonitrile
141 gradient at a flow rate of 250 nl/min. Resolution of the MS spectra was recorded at 60,000 with an
142 AGC target of 3×10^6 and a maximum injection time of 50 ms from 300 to 1,500 m/z. The 10 most
143 abundant peptide ions were selected from the MS scan and fragmented via HCD. Thereby, the
144 normalized collision energy was 27 with an isolation window of 1.6 m/z, and a dynamic exclusion of
145 30 s. MS/MS spectra were recorded at a resolution of 15,000 with an AGC target of 10^5 and a
146 maximum injection time of 50 ms. Spectra with unassigned charges, and charges of +1 and >8 were
147 excluded from the precursor selection.

148 The four datasets (lysates of pRMG and MIO-M1 cells, and secretomes of pRMG and MIO-M1
149 cells) were analyzed separately. The Proteome Discoverer 2.4 SP1 software (version 2.4.1.15;
150 Thermo Fisher Scientific) was used for peptide and protein identification via a database search
151 (Sequest HT search engine) against the SwissProt Human (MIO-M1) and Ensembl Pig (pRMG).
152 Database search was performed with full tryptic specificity, allowing for up to one missed tryptic
153 cleavage site, a precursor mass tolerance of 10 ppm, and fragment mass tolerance of 0.02 Da.
154 Carbamidomethylation of Cys was set as a static modification. Dynamic modifications included
155 deamidation of Asn and Gln, oxidation of Met, and a combination of Met loss with acetylation on
156 protein N-terminus. Peptide spectrum matches and peptides were validated with the Percolator
157 algorithm (42). Each dataset was measured as triplicate. One control sample in the dataset of MIO-
158 M1 secretomes had an unexpected low overall abundance and was excluded as an outlier. Only the
159 top-scoring hits for each spectrum were accepted with a false discovery rate (FDR) <1% (high
160 confidence). The final list of proteins satisfying the strict parsimony principle included only protein
161 groups passing an additional protein confidence filter FDR <5% filter (target/decoy concatenated
162 search validation).

163 Quantification of proteins, after precursor recalibration, was based on intensity values (at RT apex)
164 for all unique peptides per protein. Peptide abundances were normalized to the total peptide amount.
165 The protein abundances were calculated summing the normalised abundance values of corresponding
166 unique peptides. These protein abundances were used for calculation of enrichment ratios of proteins
167 in the stimulated samples to the untreated samples, resulting in single ratios for every quantified
168 protein in every treated sample. Significance of the ratios was tested using a background-based t-test
169 with correction for multiple testing according to Benjamini-Hochberg (adjusted *P*-value) (43, 44).

This is a provisional file, not the final typeset article

170 **2.5 Data analysis and visualization**

171 Calculation of the abundance ratio weight requires abundance values for both, the stimulated sample
172 and the control. However, if a protein is exclusively expressed in one of these samples, the Proteome
173 Discoverer software fails to calculate a respective abundance ratio weight. Since these extreme
174 values were of special interest to us, the missing abundance ratio weights were imputed using the R
175 package mice (version 3.13.0) and the "classification and regression trees" imputation method.

176 Ingenuity Pathway Analysis (IPA; Qiagen, Hilden, Germany) was used to analyze overrepresentation
177 of proteins in canonical pathways of the IPA library, as described elsewhere (45). IPA allows
178 deducing potential physiological effects of the various tested cytokines. Analysis was performed
179 based on the fold-change of the stimulated samples and the abundance ratio *P*-value. Fisher's exact
180 test allowed testing for nonrandom associations of proteins in the datasets and the different canonical
181 pathways (46). Furthermore, the method of Benjamini-Hochberg (B-H *P*-value) corrected for
182 multiple testing (44).

183 The euclidean distance for the heatmap analysis was calculated with the open source software Cluster
184 3.0 and hierarchically clustered by complete linkage clustering (47). The resulting heat map was
185 visualized with the open source software Java Treeview (version 1.2.0) (48).

186 **3 Results**

187 **3.1 Differential secretion of proteins after stimulation of Müller cells with various cytokines**

188 Müller cells are in close contact to all retinal cells, the vitreous and the blood vessels (17). To
189 address, whether this privileged position within the retina also translates into extensive signaling
190 between Müller cells and the surrounding cells, the secretomes of the human Müller cell-derived cell
191 line MIO-M1 and of pRMG were quantitatively analyzed by mass spectrometry after stimulation for
192 24h with the cytokines IFNγ, IL-10, IL-4, IL-6, TGFβ1, TGFβ2, TGFβ3, TNFα and VEGF,
193 respectively. By this means, we quantified 2,031 proteins in the supernatant of MIO-M1 cells (Suppl.
194 Table 1) and 3,093 proteins in the supernatant of pRMG across all treatment groups (Suppl. Table 2).

This is a provisional file, not the final typeset article

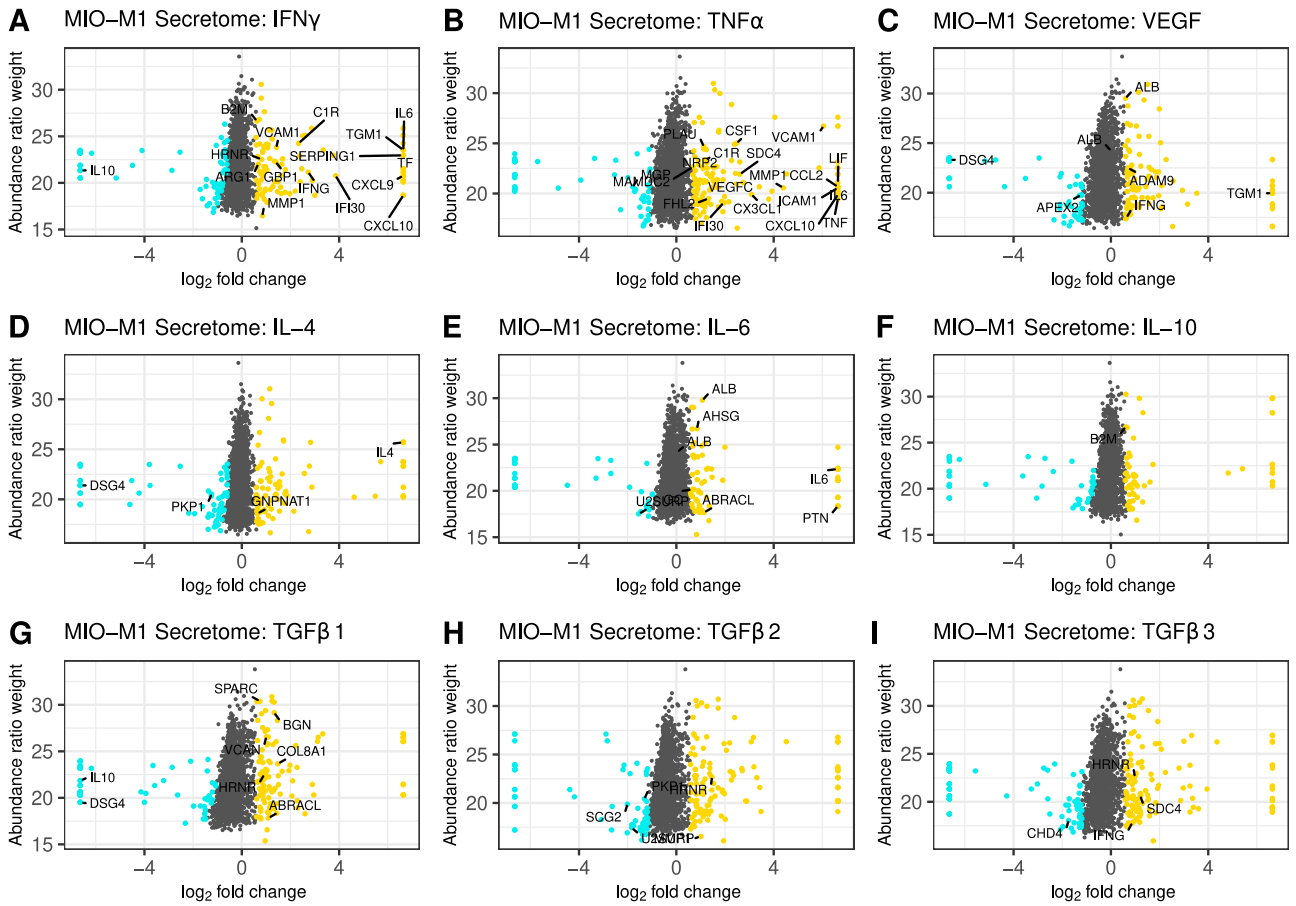

Figure 1. Scatterplot of all identified proteins from MIO-M1 secretomes after treatment with the indicated cytokines for 24 h (**A-I**). Proteins with significant changes in their abundance (±$\log_2$(1.5) fold expression, corrected p-value ≤0.05) were colored, with upregulated proteins being depicted as yellow dots, while down-regulated proteins are colored cyan. Proteins with significantly altered abundance in both, MIO-M1 and pRMG secretomes, are labeled with their gene symbol. Keratins were excluded.

Fig. 1 and Suppl. Fig. S1 summarize changes in the secretome after treatment of Müller cells with the different cytokines. A $\log_2$ fold change of ±0.58 and a corrected p-value of equal or less than 0.05 served as cutoff to define significantly upregulated or downregulated genes, respectively. Proteins equally regulated in MIO-M1 cells and pRMG were labeled with their gene symbol. However, this was only possible for proteins with identical gene symbols in the human and the porcine protein database. After treatment with IFNγ, 107 proteins in the secretome of MIO-M1 cells and 176 proteins in the secretome of pRMG were significantly more abundant, while 67 proteins of MIO-M1 cells and 96 proteins of pRMG were significantly less abundant in the supernatants (Fig. 1A; Suppl. Fig. S1A). Intriguingly, MIO-M1 cells and pRMG shared 21 upregulated and one downregulated protein. Among these shared regulated proteins after treatment with IFNγ were many with immune system functions, like signaling molecules (e.g. C-X-C Motif Chemokine Ligand 9 (CXCL9), CXCL10, IL-6) and components of the complement system (e.g. C1R, Serpin Family G Member 1 (SERPING1)). Upon treatment with TNFα, 127 (MIO-M1) or 143 (pRMG) proteins were more abundant and 57 (MIO-M1) or 87 (pRMG) proteins were less abundant in the supernatant (Fig. 1B, Suppl. Fig. S1B). Within these groups, MIO-M1 cells and pRMG shared 20 upregulated and three downregulated proteins, again with many pro-inflammatory proteins like C-X3-C Motif Chemokine Ligand 1

This is a provisional file, not the final typeset article

218 (CX3CL1), CXCL10, C-C Motif Chemokine Ligand 2 (CCL2), IL-6, and C1R being upregulated.
219 Thus, IFNγ and TNFα resulted in the most conserved changes of the secretome of Müller cells when
220 comparing between stimulated MIO-M1 cells and pRMG. In contrast, MIO-M1 cells and pRMG
221 only shared ten proteins that were more abundant and three which were less abundant after treatment
222 with VEGF, with seven proteins being keratins (Fig. 1C, Suppl. Fig. S1C). Treatment of Müller cells
223 with the three different interleukins had a subtle influence on secreted proteins with conserved
224 regulation of seven (IL-4), nine (IL-6), and two (IL-10) proteins in the secretome of MIO-M1 cells
225 and pRMG (Fig. 1D-F, Suppl. Fig. S1D-F).

226 Finally, TGFβs led to pronounced alterations in the secretome of MIO-M1 cells. TGFβ1 enhanced
227 the secretion of 125 proteins while simultaneously reducing the abundance of 67 proteins, TGFβ2
228 increased the abundance of 131 proteins while impairing secretion of 69 proteins, and TGFβ3 raised
229 abundance of 135 proteins and reduced the abundance of 76 proteins (Fig. 1G-I). Furthermore, eleven
230 proteins of MIO-M1 cells and pRMG were similarly regulated by TGFβ1, eight upregulated and
231 three downregulated (Suppl. Fig. S1G). After treatment with TGFβ2, three proteins were more
232 abundant and four proteins less abundant in the secretome of both cell types (Suppl. Fig. S1H).
233 Additionally, the secretome of TGFβ3 treated MIO-M1 cells and pRMG shared one downregulated
234 protein and eight upregulated proteins, with most proteins like Osteonectin (Secreted Protein Acidic
235 And Rich In Cysteine; SPARC), Matrix Metallopeptidase 1 (MMP1), Biglycan (BGN) and various
236 keratins being functionally related to extracellular matrix organization (Suppl. Fig. S1I).
237 Furthermore, stimulation with TGFβ3 evoked upregulation of pro-inflammatory cytokine IFNγ in
238 both, the MIO-M1 cell line and pRMG. Overall, there are subtle, but intriguing differences in protein
239 abundances after stimulation of Müller cells with the different TGFβ isoforms. Some of the proteins
240 differentially induced by the TGFβ isoforms in MIO-M1 cells are pro-inflammatory cytokines, like
241 IFNγ, TNFα, and CCL2 (Suppl. Table 1).

This is a provisional file, not the final typeset article

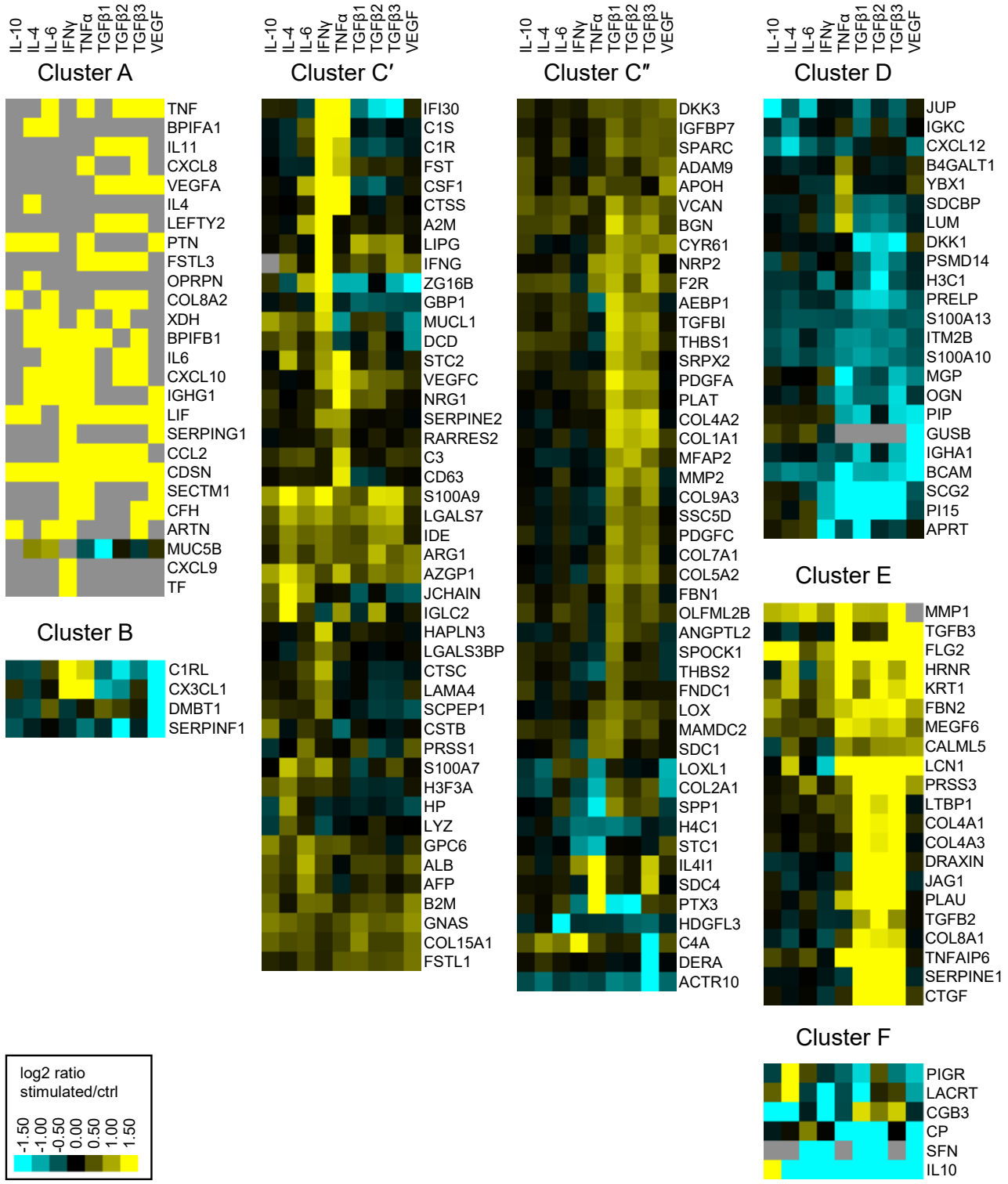

Figure 2. Heatmap of hierarchical cluster analysis of proteins secreted by MIO-M1 cells after treatment with various cytokines. Identified proteins were filtered for extracellular proteins with significant changes in expression ($\pm\log_2(1.5)$ fold expression, corrected p-value ≤ 0.05). Down-regulated proteins are presented in cyan, while up-regulated proteins are depicted yellow for the respective treatments. Gray squares represent proteins that were neither identified in the

This is a provisional file, not the final typeset article

untreated control, nor in the respective treatment. Clusters were defined using the branches of a dendrogram and shown as close up with the corresponding gene symbols.

Next, we aimed to examine the physiological functions of proteins secreted by Müller cells. Therefore, we ordered secreted proteins in distinct clusters, grouped by similar expression patterns. From the identified proteins of the MIO-M1 supernatant, all cytosolic contaminants were removed, resulting in a list that exclusively contained extracellular proteins. Furthermore, only those proteins that showed a significant change of abundance (corrected p-value ≤ 0.05 and $\pm$ 1.5-fold abundance) in at least one treatment were selected for further analysis. As a result, a hierarchical heat map and an associated dendrogram consisting of 171 proteins was generated using the $\log_2$ abundance ratio of treated and untreated control cells (Suppl. Fig. S2). Furthermore, clusters were highlighted depending on their position on the dendrogram (Fig. 2). To avoid single protein clusters, the proteins Polymeric Immunoglobulin Receptor (PIGR) and Lacritin (LACRT) were assigned to Cluster F, despite being on different branches of the dendrogram.

Notably, we identified proteins which were secreted by MIO-M1 cells exclusively after stimulation (cluster A), while another set of proteins was completely absent in MIO-M1 cells (cluster B) treated with VEGF. The largest cluster comprises proteins upregulated by at least one cytokine (cluster C). In contrast to cluster D, consisting of proteins downregulated by TGFβs, TGFβs induce secretion of proteins of cluster E. Finally, secretion of most proteins of cluster F is deterred by at least one cytokine.

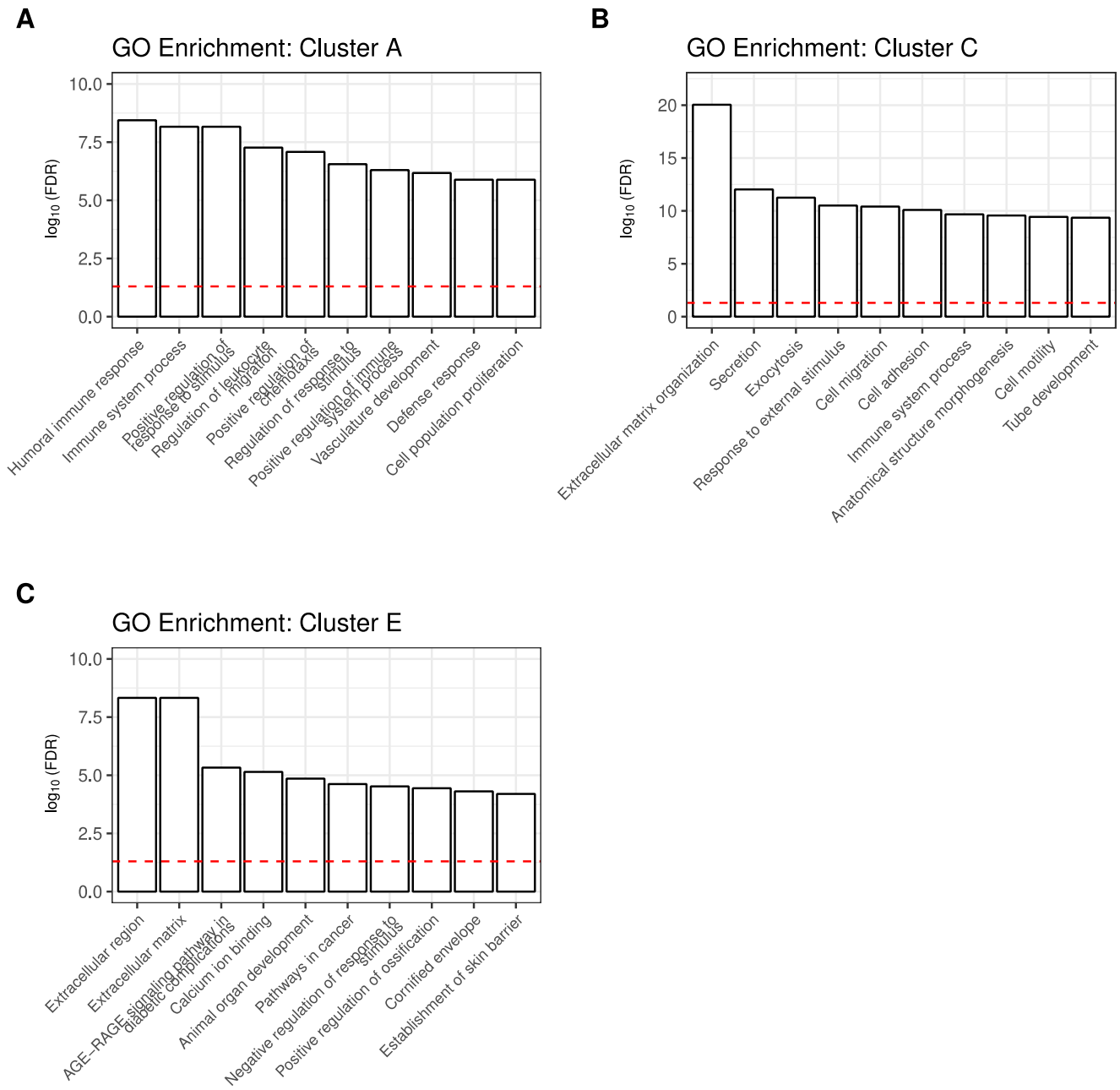

Figure 3. A shiny GO enrichment analysis for the previously defined cluster A (**A**), cluster C (**B**) and cluster E (**C**) was performed. Redundant pathways were reduced to show only one representative pathway. Depicted is the –log10(FDR) of the top 10 pathways for each cluster. The red dashed line indicates the significance threshold.

The clusters A, C and E are large clusters with proteins upregulated by at least one cytokine, with cluster A being the cluster with the most pronounced changes in secretion of its members and cluster C being the most diffuse one. In order to deduce the physiological functions of the secreted proteins of each of these clusters, we performed gene ontology (GO) analysis. Thereby, redundant pathways were condensed to a single representative pathway and the top 10 pathways with the lowest enrichment FDR were displayed. Intriguingly, the top 10 pathways for cluster A were related to

This is a provisional file, not the final typeset article

immune system processes, with "Humoral immune response" and "Immune system process" being the most significant pathways with an enrichment FDR of 3.6×10^{-9} and 6.9×10^{-9}, respectively (Fig. 3A). Furthermore, cluster C contained the pathway "Immune system process", while most other pathways in this cluster C were involved in shaping the extracellular environment (Fig. 3B). Besides further pathways involved in extracellular remodeling, the proteins of cluster E were also associated to the pathway "AGE-RAGE signaling pathway in diabetic complications" (Fig. 3C).

3.2 In-depth analysis of the Müller cell proteome after stimulation with a selection of cytokines

Our secretome analysis hints towards extensive signaling between Müller cells and their cellular environment, differentially induced by various cytokines. To elucidate the underlying cellular alterations, we also investigated differences in the proteome of MIO-M1 cells and pRMG cells by mass spectrometry after treatment with these cytokines for 24 h. In total, 5,514 proteins were quantified in the lysates of MIO-M1 cells (Suppl. Table 3) and 4,187 proteins in the lysates of pRMG cells (Suppl. Table 4) across all treatment groups.

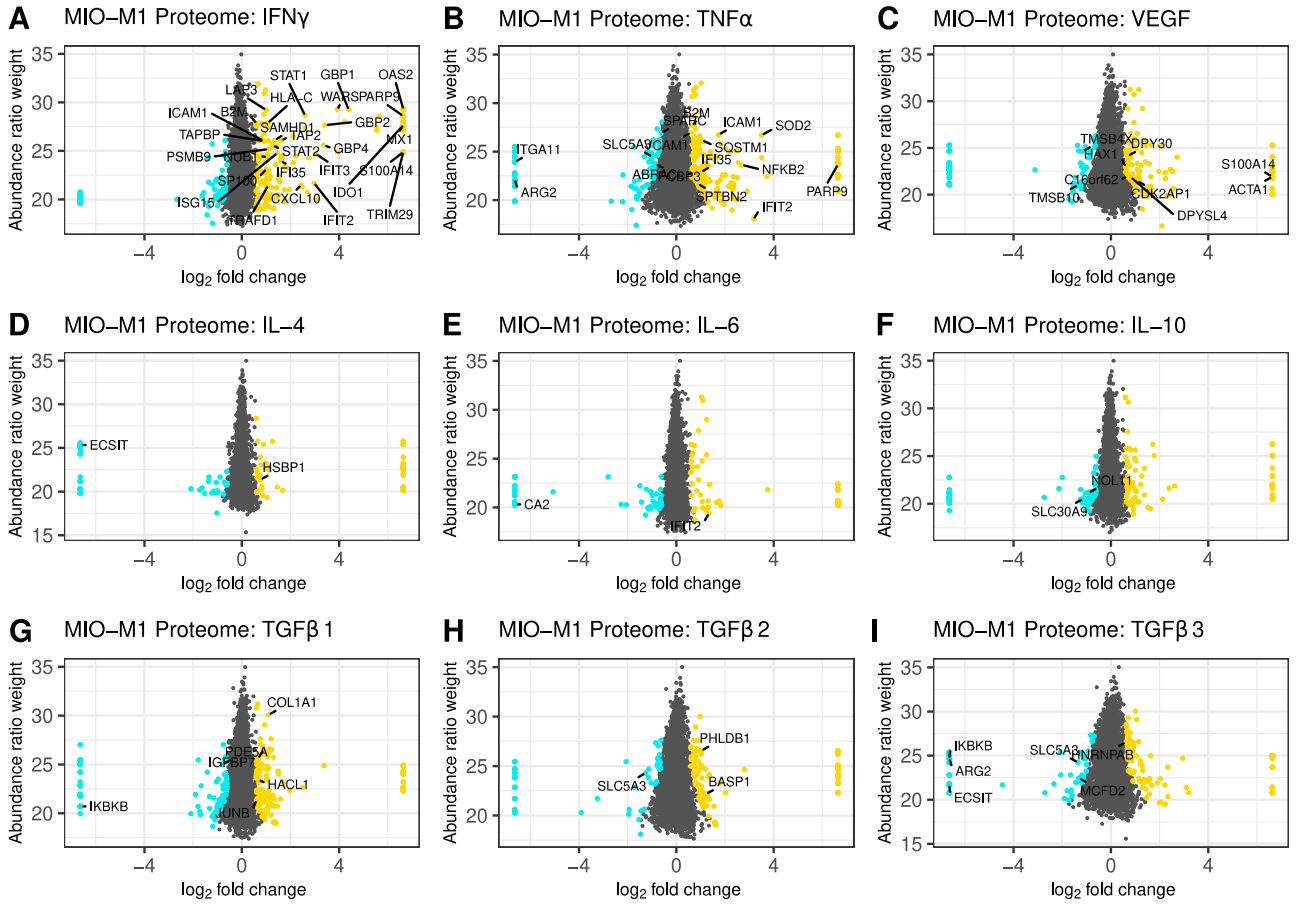

Figure 4. Scatterplot of all identified proteins from MIO-M1 lysates after treatment with the indicated cytokines for 24 h (**A-I**). Proteins with significant changes in their abundance ($\pm\log_2(1.5)$ fold expression, corrected p-value ≤ 0.05) were colored, with upregulated proteins being depicted as yellow dots, while down-regulated proteins are colored cyan. Proteins with

297 significantly altered abundance in both, MIO-M1 and pRMG lysates, are labeled with their
298 gene symbol. Keratins were excluded.

299 The threshold for significant abundance changes was set using the same cutoff values as for the
300 secretome, and equally regulated proteins in MIO-M1 cells and pRMG were labeled with their gene
301 symbol, if they shared the same gene symbol in the human and the porcine database (Fig. 4; Suppl
302 Fig. S3). Although the porcine protein database contains mostly humanized gene symbols, the swine
303 leukocyte antigens (SLA) genes show little sequence homology between the human and the porcine
304 genome and cannot properly be humanized (49). However, Human Leukocyte Antigen-C Alpha
305 Chain (HLA-C) was part of the porcine protein database.

306 Treatment of Müller cells with IFNγ resulted in 206 more abundant and 88 less abundant proteins in
307 MIO-M1 cells and 331 more abundant and 36 less abundant proteins in pRMG lysates (Fig. 4A;
308 Suppl Fig. S3A). Thereof, 29 proteins showed higher expression levels in both cells types. Among
309 the overlapping proteins were restriction factors like SAM And HD Domain Containing
310 Deoxynucleoside Triphosphate Triphosphohydrolase 1 (SAMHD1) and MX Dynamin Like GTPase
311 1 (MX1), transcription factors like Signal Transducer And Activator Of Transcription 1 (STAT1) and
312 STAT2, regulators of protein homeostasis like Leucine Aminopeptidase 3 (LAP3) or the Proteasome
313 20S Subunit Beta 9 (PSMB9), and proteins associated with peptide transport and antigen presentation
314 like Transporter 2, ATP Binding Cassette Subfamily B Member (TAP2), TAP Binding Protein
315 (TAPBP), Beta-2-Microglobulin (B2M), as well as HLA-C. After treatment with TNFα, 204 proteins
316 were more abundant in the proteome of MIO-M1 cells, while 119 proteins were less abundant (Fig.
317 4B). In pRMG, 207 proteins with higher abundance and 285 proteins with lower abundance were
318 identified upon treatment with TNFα, with 18 proteins that were differentially regulated in both cell
319 types (Suppl. Fig. S3B). Among shared proteins that were more abundant after treatment with TNFα
320 were pro-inflammatory proteins like B2M and Nuclear Factor Kappa B Subunit 2 (NFKB2), or
321 adhesion molecules like Intercellular Adhesion Molecule 1 (ICAM1) or Vascular Cell Adhesion
322 Molecule 1 (VCAM1). VEGF led to 143 more and 102 less abundant proteins in MIO-M1 cells or
323 232 more and 224 less abundant proteins in pRMG, respectively (Fig. 4C; Suppl. Fig. S3C). Thereof,
324 MIO-M1 cells and pRMG shared nine more abundant proteins, inter alia proteins associated with
325 reorganization of the cortical cytoskeleton like Alpha-Actin-1 (ACTA1) or HCLS1 Associated
326 Protein X-1 (HAX1), and two less abundant proteins, Thymosin Beta 10 (TMSB10) and Thymosin
327 Beta 4 X-Linked (TMSB4X), both inhibitors of actin polymerization. Upon treatment with
328 interleukins IL-4, IL-6 and IL-10, the Müller cell proteomes mirrored the subtle effects of these
329 cytokines on the abundance of proteins observed for the Müller cell secretomes (Fig. 4D-F, Suppl.
330 Fig. S3D-F). Also in line with the secretome data, the overlap between differentially abundant
331 proteins of the MIO-M1 and pRMG proteome after treatment with the various interleukins contained
332 only few proteins. In contrast, TGFβ1 increased the abundance of 143 proteins, while decreasing the
333 abundance of 94 proteins in the proteome of MIO-M1 cells and increased the abundance of 203
334 proteins, while decreasing the abundance of 103 proteins in the proteome of pRMG (Fig. 4G; Suppl.
335 Fig. S3G). In comparison to the lower abundant proteins Phosphodiesterase 5A (PDE5A) and
336 Inhibitor Of Nuclear Factor Kappa B Kinase Subunit Beta (IKBKB), the proteins Collagen Type I
337 Alpha 1 Chain (COL1A1), Insulin Like Growth Factor Binding Protein 7 (IGFBP7), JunB Proto-
338 Oncogene (JUNB), and 2-Hydroxyacyl-CoA Lyase 1 (HACL1) were more abundant in both, MIO-
339 M1 cells and pRMG after treatment with TGFβ1. Following treatment with TGFβ2, 125 proteins of
340 the proteome of MIO-M1 cells and 266 proteins of the proteome of pRMG were more abundant,
341 whereas 67 proteins of the MIO-M1 proteome and 229 proteins of the pRMG proteome were less
342 abundantly expressed (Fig. 4H; Suppl. Fig. S3H). In the case of treatment with TGFβ3, 130 proteins
343 in the MIO-M1 proteome and 185 in the pRMG proteome showed higher abundances, while 94

This is a provisional file, not the final typeset article

344 proteins in MIO-M1 proteome and 250 in the pRMG proteome were less abundant (Fig. 4I; Suppl.
345 Fig. S3I). The overlap of MIO-M1 cells and pRMG treated with TGFβ2 comprised three proteins,
346 and treatment with TGFβ3 resulted in an overlap of seven proteins. Overall, pRMG reacted more
347 pronounced to treatment with the various cytokines compared to MIO-M1 cells.

348 **3.3 Canonical pathways enriched in Müller cells upon stimulation**

349 Treatment with various cytokines partly induced pronounced changes in the secretome and proteome
350 of Müller cells. In the secretome, these changes primarily included the secretion of pro-inflammatory
351 cytokines and proteins associated with organization of the extracellular matrix. To elucidate
352 overrepresented mechanisms and pathways in stimulated Müller cells, we performed Ingenuity
353 pathway analysis (IPA). We limited the IPA to significantly regulated proteins (p-value ≤ 0.05)
354 identified in the MIO-M1 and pRMG lysates. Since IPA cannot handle porcine gene symbols, we
355 replaced the only canonical SLA gene SLA-1 in our pRMG dataset by the canonical human HLA
356 gene HLA-A. Hence, an IPA core analysis was performed with 1,543 proteins for pRMG and with
357 2,262 proteins for the MIO-M1 cells. IPA identified 338 canonical pathways within the proteome of
358 MIO-M1 cells and 218 canonical pathways in the proteome of pRMG that were significantly
359 enriched by at least one of the used cytokines (IPA p-value ≤ 0.05; Suppl. Table 5). Among the
360 identified canonical pathways were many pathways associated with signaling, cell death, immune
361 system processes and the cellular redox state (Fig. 5; Suppl. Fig. S4). A selection of canonical
362 pathways enriched in both pRMG and MIO-M1 cells after treatment with at least one of the tested
363 cytokines is depicted in Fig. 5.

This is a provisional file, not the final typeset article

Figure 5. A comparative IPA analysis with the significantly regulated proteins identified in the pRMG lysates after stimulation with the indicated cytokines was performed. Canonical pathways related to signaling, cell death, immune system processes and oxidative stress were selected. Pathways with significant enrichment of genes after stimulation with at least one cytokine are presented. Significance of the gene enrichment for each pathway and treatment is indicated by purple squares in the left array. Thereby, treatments that did not meet the

This is a provisional file, not the final typeset article

371 significance threshold (p-value ≤ 0.05) are marked with a dot. The z-score is indicated in the
372 right array and represents a prediction of activation (orange) or inhibition (blue) of the
373 pathway. Gray squares mark treatments where the activation state of a pathway could not be
374 calculated.

375 Among the most significantly regulated pathways in MIO-M1 cells and pRMG were the canonical
376 pathways "Mitochondrial Dysfunction" and "Oxidative Phosphorylation". These pathways were
377 significantly induced by all examined cytokines in pRMG. The pathways "Ferroptosis Signaling
378 Pathway", "iNOS Signaling", "NRF2-mediated Oxidative Stress Response", and "Production of
379 Nitric Oxide and Reactive Oxygen Species in Macrophages" are closely linked to the cellular redox
380 state and were among the enriched pathways in MIO-M1 cells and pRMG after treatment with
381 various cytokines. Furthermore, proteins associated with the maturation of phagosomes were
382 significantly enriched in pRMG. In line with this, "Caveolar-mediated Endocytosis Signaling" was
383 significantly enriched in pRMG after treatment with IFNγ, TGFβ1, TNFα and VEGF, and "Clathrin-
384 mediated Endocytosis Signaling" was significantly enriched in pRMG after treatment with all
385 cytokines except IL-10. Besides these two pathways associated with the recycling of the extracellular
386 environment, intracellular protein homeostasis and MHC class I peptide generation was facilitated by
387 enrichment of the "Protein Ubiquitination Pathway" in pRMG after treatment with IFNγ, TGFβ3,
388 TNFα and VEGF. Similarly, IFNγ, IL-4, TGFβ1, TGFβ3, TNFα and VEGF enriched "Protein
389 Ubiquitination Signaling" in MIO-M1 cells. "Neuroinflammation Signaling" was induced by IFNγ,
390 TNFα and VEGF in MIO-M1 cells and by IFNγ, TGFβ1, TGFβ3 and TNFα in pRMG, whereas
391 TGFβ2 and VEGF led to a slight inhibition of this pathway in pRMG.

392 **3.4 A deeper look into Müller cell complement secretion upon cytokine stimulation**

393 Because the enrichment analysis of the secretome yielded highly significant hits such as "humoral
394 immune response" and "immune system process," we took a closer look at complement proteins in
395 the secretome and cell lysates. Notably, most complement proteins are secreted as key components of
396 the humoral immune system. The identified complement components include central complement
397 proteins, regulators, and receptors. Consistent with their localization in the cell membrane, the latter
398 (including ITGAM, ITGB2, C5aR1) were detected only in cell lysates, and here specifically in those
399 of pRMGs. The complement regulators clusterin (CLU), vitronectin (VTN), CD59, and SERPING
400 were found in most test samples. With regard to the central complement components, the pRMG
401 secretome took a prominent position and showed results for complement components for all three
402 different activation pathways (e.g. C1q, FD, MASP1) and the terminal pathway (e.g. C9). The central
403 complement protein C3 was found in both the MIO-M1 and pRMG secretomes and in the MIO-M1
404 lysate. Interestingly, cytokine treatment induced changes in complement proteins and regulators but
405 had no effect on complement receptor expression. We observed that C1q subunits, which initiate the
406 classical complement pathway by binding to antibodies, were detectable only in pRMG but not in
407 MIO-M1 cells. C1q levels in cell lysates and the corresponding secretome were consistently reduced
408 after TNFα treatment but were increased by IFNγ. Moreover, complement proteases C1r and C1s,
409 which bind to C1q therewith continuing the cascade of classical pathway activation, were enriched in
410 the supernatants of MIO-M1 and pRMG cells treated with IFNγ (Fig. 2C). In contrast, C1r
411 concentration was significantly decrease in supernatants of MIO-M1 cells but not pRMG after VEGF
412 and TGFβ2 application. Notably, C1s and C1r were not detected in cellular lysates. Interestingly, the
413 abundance of the central complement proteins C3 and C4A were modified by the supplemented
414 cytokines in MIO-M1 secretomes only and not in any other data set (Fig. 2C). These proteins are
415 cleaved upon complement activation as for example triggered by the C1q-mediated classical pathway
416 and result in cleaved products which interact with cellular receptors (e.g. C3a/C3b, C4a). Here,

417 complement protein C3 is mainly increased following TNFα addition and C4 upon exposure to IFNγ
418 (Fig. 2C). In fact, IFNγ was also the major player modulating the secreted complement components
419 in pRMG: C2 and FI were significantly increased while C9, FD and MASP1 were clearly reduced in
420 its presence. These complement components absent from any other sample.

421 Regarding the complement regulators factor H (FH), SERPING and CLU are of interest. Secretion of
422 FH was not observed in untreated MIO-M1 and pRMG, but it was significantly upregulated in MIO-
423 M1 secretomes following IFNγ, TNFα, TGFβ3, and VEGF treatment (Fig. 2A). Similar results were
424 obtained for SERPING, whose levels were increased by IFNγ in the MIO-M1 secretome, pRMG cell
425 lysates and secretome. Remarkably, the MIO-M1 lysate showed decreased values for CLU following
426 IFNγ, TGFβ1 and TNFα, and similar but not significant trends was observed for the respective
427 secretome. Finally, while CLU was upregulated in pRMGs lysates upon IL-6 or VEGF treatment, no
428 significant alterations could be found in corresponding secretomes.

429 In summary, IFNγ and TNFα seemed to be the most effective cytokines to modulate the Müller cell
430 complement expression and secretion (Fig. 2).

431 **3.5 Müller cells as atypcial antigen-presenting cells**

432 Intriguingly, treatment of pRMG with IFNγ, TGFβ2, TGFβ3 and TNFα significantly enriched
433 proteins associated with the "Antigen Presentation Pathway". Likewise, the "Antigen Presentation
434 Pathway" was induced in MIO-M1 cells by treatment with IFNγ, TGFβ1, TNFα and VEGF. Thereby,
435 antigen presentation is an umbrella term for two distinct processes. MHC class I antigen presentation
436 is common to all nucleated cells and allows $CD8^+$ cytotoxic T cells (CTL) to assess whether cells are
437 infected with an intracellular pathogen (50, 51). In contrast, MHC class II is presented to antigen
438 specific $CD4^+$ T cells mainly by professional antigen-presenting cells inducing their activation and
439 differentiation to T helper cells (52).

This is a provisional file, not the final typeset article

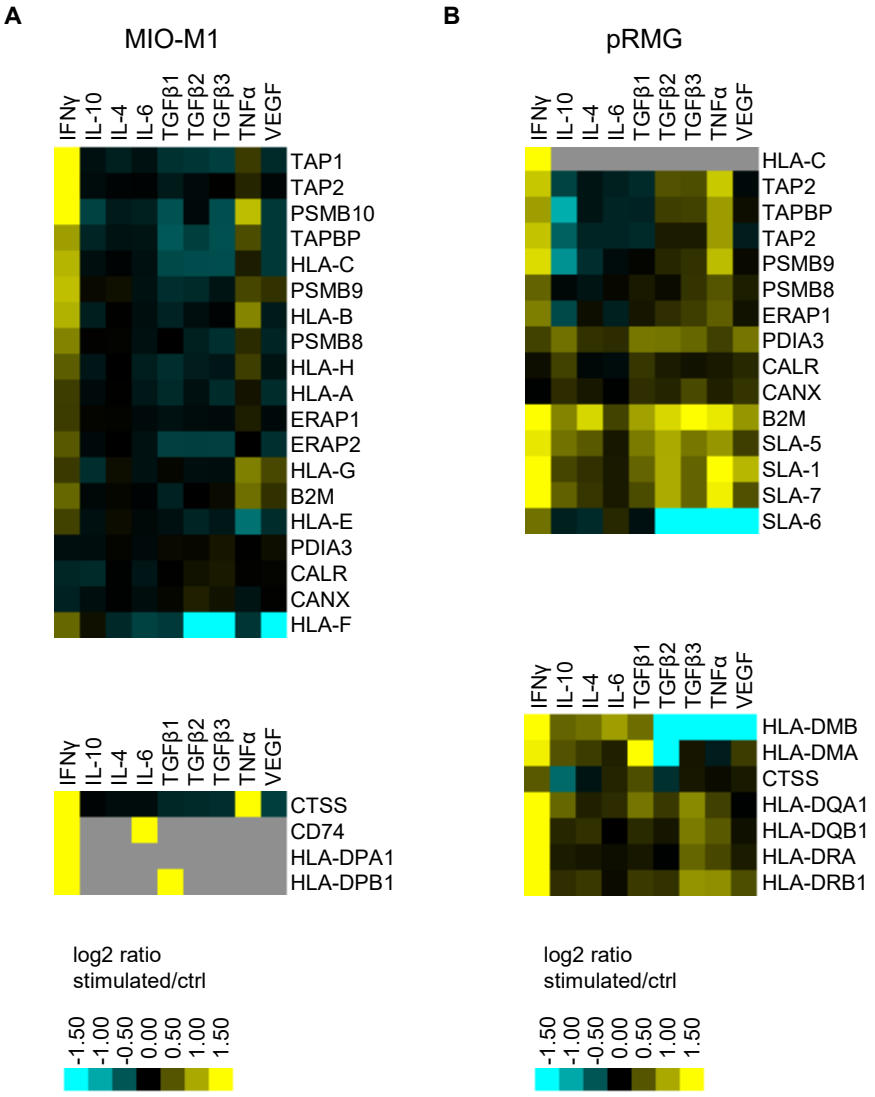

Figure 6. Heatmap of hierarchical cluster analysis of proteins involved in MHC class I (upper panel) and MHC class II (lower panel) antigen presentation expressed by MIO-M1 cells (**A**) and pRMG cells (**B**) after treatment with various cytokines. Down-regulated proteins are presented in cyan, while up-regulated proteins are depicted yellow for the respective treatments. Gray squares represent proteins that were neither identified in the untreated control, nor in the respective treatment. The heatmap was generated on the basis of the $\log_2$ fold change of the respective proteins.

To investigate the antigen presentation capacity of Müller cells, we constructed a hierarchical heatmap for MIO-M1 cells (Fig. 6A) and pRMG (Fig. 6B) challenged with various cytokines. Proteins linked to antigen presentation were selected and clustered hierarchically. Proteins associated with MHC class I antigen presentation are displayed in the upper panel and proteins correlated to MHC class II antigen presentation are depicted in the lower panel. In MIO-M1 cells, IFNγ induced the majority of proteins linked to both, MHC class I and II antigen presentation, whereas TNFα exerted its inductive effect exclusively on MHC class I antigen presentation. The only protein linked to MHC class II antigen presentation induced by TNFα in MIO-M1 cells was Cathepsin S (CTSS). Furthermore, the other cytokines did not induce proteins related to antigen presentation in MIO-M1 cells. Quite the contrary, TGFβ2 and TGFβ3 reduced the abundance of proteins linked to MHC class

I antigen presentation in these cells. In contrast to MIO-M1 cells, pRMG reacted to all tested cytokines by induction of components of both MHC class I and II antigen presentation to varying degrees. IFNγ and TNFα induced proteins of MHC class I and II antigen presentation in pRMG, among others SLA-DQA1, SLA-DQB1, SLA-DRA and SLA-DRB1. Furthermore, class I and II antigen presentation was upregulated by TGFβ isoforms 1-3 in pRMG. While TGFβ2 and TGFβ3 induced the components of the MHC class I peptide loading complex TAP2 and TAPBP, TGFβ1 also increased the abundance of HLA-DMA and HLA-DMB, proteins involved in the peptide loading on MHC class II. We saw only a subtle induction of proteins related to antigen presentation by IL-10, IL-4 and IL-6. The smallest impact on antigen presentation proteins was seen after stimulation with IL-6. Furthermore, IFNγ significantly upregulated the expression of the co-stimulatory molecule CD40 in pRMG, while TGFβ2, TGFβ3, TNFα and VEGF resulted in lower abundance of CD40 (Suppl. Table 4).

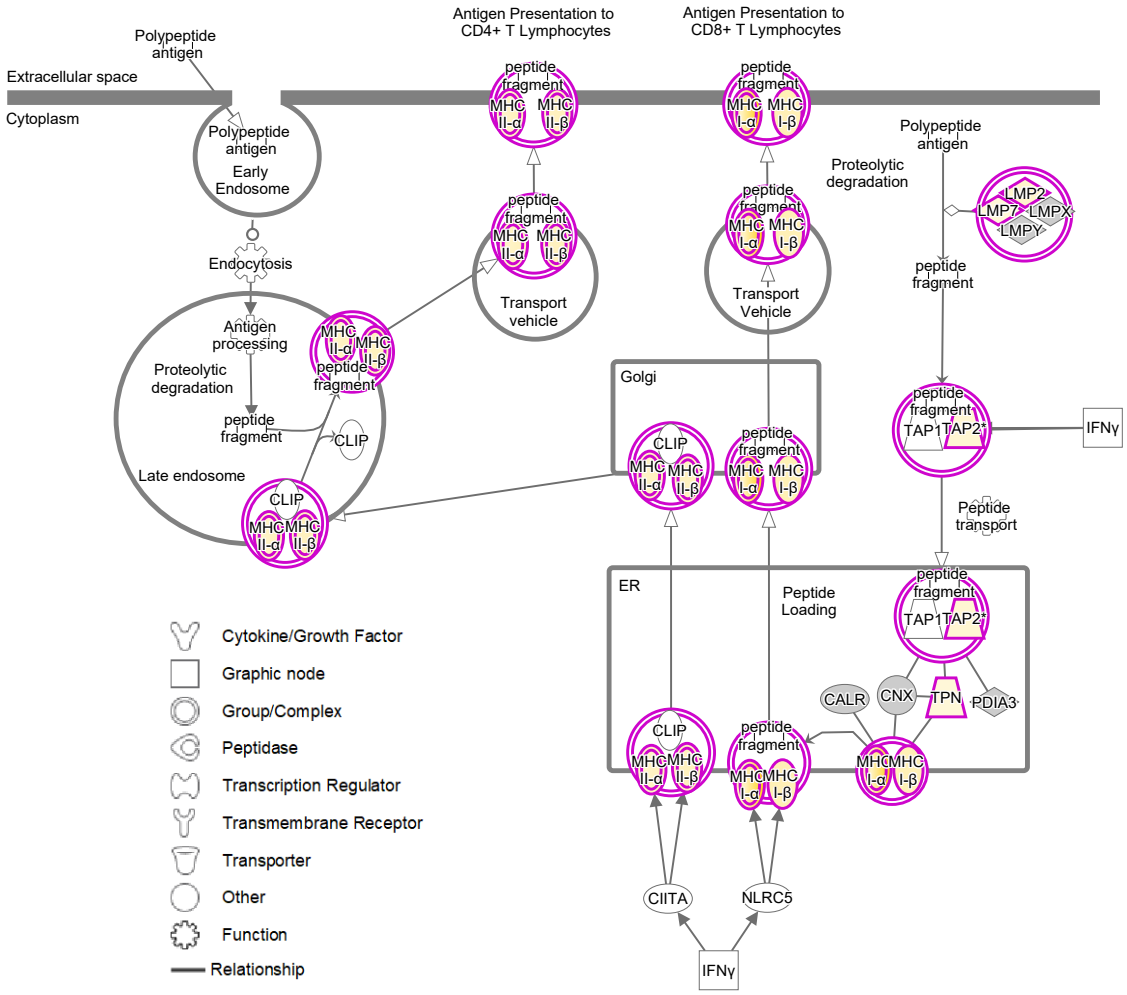

Figure 7. IPA for pRMG cells after treatment with IFNγ was performed. Depicted is the canonical antigen presentation pathway. Yellow proteins are induced. The intensity of the yellow color indicates the degree of upregulation. Grey proteins are in the dataset but did not

This is a provisional file, not the final typeset article

474 pass the analysis cutoffs of the pathway analysis. Purple circles highlight proteins (single
475 circle) or complexes (double circles).

476 Induction of the canonical MHC class I and MHC class II antigen presentation pathway as assessed
477 by IPA for pRMG after treatment with IFNγ is summarized in Fig. 7. This pathway was enriched in
478 pRMG cells with a p-value of 4.15×10^{-12}. Besides MHC class I and MHC class II, also components
479 of the peptide loading complex of MHC class I (TAP2 and TPN) were upregulated in pRMG after
480 IFNγ treatment. Furthermore, IFNγ induces the Large Multifunctional Peptidase 2 (LMP2;
481 synonymous to PSMB9) and Large Multifunctional Peptidase 7 (LMP7; synonymous to PSMB8)
482 subunits of the immunoproteasome in MIO-M1 cells.

483 **4 Discussion**

484 DR is a condition associated with microvascular degeneration, resulting in ocular inflammation and
485 eventually in complete blindness (53). As the prevalence of diabetes in developed and developing
486 countries rises, DR became the leading cause of blindness in the working-age population (54).
487 Microglia are resident innate immune cells in the retina and as such, they are considered to regulate
488 the inflammation during DR (55). In contrast, the role of Müller cells during the pathology of DR has
489 been often described to be the metabolic support of neurons (53) . However, growing evidence
490 suggests excessive signaling between Müller cells and the surrounding tissue including microglia,
491 with both beneficial and detrimental consequences for the pathogenesis of DR (56). We show here
492 that stimulation of Müller cells with pro-inflammatory cytokines like IFNγ or TNFα, but also with
493 growth factors like TGFβ or VEGF resulted in profound, yet distinct response profiles in their
494 secretomes, thus confirming their central role in cell-to-cell communication within the retina.

495 Previously, it has been shown that the conditional knock-out of VEGF in Müller cells of mice
496 reduced the expression of inflammatory markers like TNFα or ICAM1 compared to diabetic control
497 mice, indicating a pro-inflammatory effect of VEGF on Müller cells (57, 58). Here we could show
498 that VEGF induced the Müller cell line MIO-M1 to secrete proteins associated with immune effector
499 processes like IFNγ, B2M, HRNR, and complement-associated proteins like SERPING1 and
500 complement factor H (FH). Furthermore, ICAM1 was more abundant in our proteome data of MIO-
501 M1 cells and pRMG treated with VEGF compared to the respective control cells. Thus, we were able
502 to confirm the pro-inflammatory role of VEGF in Müller cells.

503 Overall, we observed that MIO-M1 cells secreted TNFα upon stimulation with VEGF, IL-6, and the
504 TGFβ isoforms 2 and 3. Increased levels of TNFα were previously identified in the vitreous of DR
505 patients (59). Furthermore, Müller cells have been reported to secrete increased amounts of VEGF
506 and TNFα under stress conditions like inflammation or hyperglycemia, thereby promoting retinal
507 inflammation (57, 60-64). Our results show that TNFα induced MIO-M1 cells to secrete
508 inflammatory proteins but also proteins associated with tissue development like Leukemia Inhibitory
509 Factor (LIF), Follistation (FST), Neuregulin 1 (NRG1), or Pleiotrophin (PTN), to name but a few.
510 Thus, our data suggest a pleotropic role of TNFα in Müller cells.

511 TGFβs regulate early embryogenesis, maintenance and regeneration of mature tissues, and various
512 disease processes (65). TGFβ1 has been described to be anti-inflammatory, inducing immune
513 tolerance in the periphery and preventing autoimmunity. Thus, knock out of TGFβ1 in mice induced
514 autoantibodies and multifocal inflammatory disease in many tissues, eventually causing the mice to
515 die within 4 weeks of age (66). In our *in vitro* model, treatment of MIO-M1 cells with TGFβ1
516 induced secretion of CCL2 and therefore might result in the recruitment of leukocytes.

517 Simultaneously, TGFβ1 enhanced the secretion of anti-inflammatory proteins like TNF Alpha
518 Induced Protein 6 (TNFAIP6) or LIF in Müller cells. In contrast, TGFβ2 and TGFβ3 also promoted
519 immune system processes in MIO-M1 cells by inducing secretion of pro-inflammatory cytokines
520 TNFα, CXCL8, CXCL10 and IFNγ. It has been shown that TGFβ2 acts immunomodulatory in
521 aqueous humor by decreasing the expression of IL-6, CXCL1, CCL2, G-CSF and IGFBP-5 (67).
522 However, we demonstrated that treatment of Müller cells with TGFβ2 induced expression of IL-6
523 and CCL2, suggesting a complex and diverse role of TGFβ2 signaling in the eye. Although TGFβ
524 isoforms are closely related (sharing 71-79% sequence identity), have similar three-dimensional
525 structures and signal canonically through the same receptor (68), our secretome analyses provide
526 evidence that they affect Müller cells differentially. While knock-out of the TGFβ isoforms resulted
527 in different phenotypes, all null mutations were lethal (69-72). Replacement of the coding sequences
528 by one of the other isoforms only partially rescued these phenotypes, implying intrinsic differences
529 of these isoforms (73, 74). These differences might originate from varying flexibilities of an
530 interfacial helix and thus modify the binding of the TGFβ isoforms to matrix proteins as suggested by
531 Huang and colleagues (68). Latent TGFβ binds Thrombospondin 1 (THBS1), augmenting its
532 activation (75-77). Intriguingly, in our study, all three TGFβs elevate the abundance of THBS1
533 indicating a positive feedback loop. Recently, transcriptome analysis linked the expression of TGFβ
534 isoforms of mice to activation of different signaling cascades. While TGFβ1 and TGFβ2 evoked the
535 non-canonical p38MAPK signaling pathway, which has been linked to gliosis, TGFβ3 induced the
536 SMAD canonical signaling pathway for TGFβs in mice (78, 79). During glaucoma, the aqueous
537 humor contains elevated levels of TGFβ2, exceeding levels for homeostatic signaling (77, 80).
538 Thereby, TGFβ2 has been associated with pathological remodeling of the trabecular meshwork and
539 the optical nerve head (77). Furthermore, it stimulated secretion of extracellular matrix proteins by
540 astrocytes and cells of the lamina cribrosa (81-84). Our data suggest that Müller cells also contribute
541 to the remodeling of the extracellular matrix as stimulation with TGFβ1 and TGFβ3 resulted in
542 enhanced secretion of extracellular matrix proteins like Fibrillin-2 (FBN2), various keratins, and
543 collagens. Furthermore, they simultaneously enhanced the turnover of extracellular matrix by
544 inducing the secretion of the Matrix Metalloprotease-1 (MMP1) and MMP2. Previously, MMP2 has
545 been described to be elevated in DR patients and to promote the pathogenesis of DR by inducing
546 mitochondrial dysfunction and apoptosis of retinal capillary cells (85). Intriguingly, our IPA also
547 indicates that the canonical pathway for mitochondrial dysfunction is enriched in Müller cells upon
548 stimulation with all TGFβ isoforms. However, this is not solely due to the enhanced secretion of
549 MMP2, since mitochondrial dysfunction is enriched in Müller cells by all tested cytokines, whereas
550 TGFβs exclusively induce MMP2.

551 A meta-analysis of eleven studies recently showed significantly increased levels of the anti-
552 inflammatory cytokine IL-10 in the vitreous humor of DR patients (86). Moreover, IL-10 levels were
553 higher in patients with proliferative DR compared to patients with non-proliferative DR (86). While
554 our data show no contribution of Müller cells to elevated IL-10 secretion upon stimulation with the
555 tested cytokines, IL-10 induced proteins associated with tissue development, cell adhesion, and
556 angiogenesis in MIO-M1 cells, namely Corneodesmosin (CDSN), LIF, PTN, and various collagens,
557 to name a few. In line with this, it has been shown that IL-10 is involved in the pathological
558 angiogenesis during the development by modulating the macrophage response to hypoxia (87). Thus,
559 we hypothesize that IL-10 might also be involved in the abnormal angiogenesis during DR.

560 Previously, it has been shown that the canonically anti-inflammatory IL-4 can potentiate cytokine
561 and chemokine production in macrophages following a pro-inflammatory stimulus (88-90). In line
562 with this, we observed increased abundances of many pro-inflammatory proteins like IFNγ, S100A9,
563 S100A7, CXCL10, and Lysozyme C (LYZ) upon stimulation of MIO-M1 cells with IL-4, indicating

This is a provisional file, not the final typeset article

564 that IL-4 does not exert an anti- but a pro-inflammatory influence in these cells. Interestingly, MIO-
565 M1 cells did not secrete the anti-inflammatory interleukin IL-4 upon treatment with the various tested
566 cytokines. Secretion of pro-inflammatory IL-6 by Müller cells has been described upon treatment
567 with IL-1β or LPS (91). Furthermore, elevated levels of IL-6 were found in the vitreous and serum of
568 DR patients and even further increased in patients suffering from proliferative DR (92). Here we
569 show that IFNγ, TNFα, TGFβ2, and TGFβ3 also induced the secretion of IL-6 in MIO-M1 cells.
570 Previously, it was shown that IL1β induced IL-6 through activation of the p38MAPK signaling
571 pathway (93). The murine TGFβ isoforms 1 and 2 also activated the p38MAPK signaling in Müller
572 cells of mice (78). Thus, the involvement of p38MAPK signaling in secretion of IL-6 by Müller cells
573 should be addressed in further studies. Brandon and colleagues demonstrated induction of VEGF by
574 IL-6 in Müller cells, especially under hyperglycemic conditions, preventing Müller cells from
575 glucose toxicity (94). In contrast, our analysis revealed no VEGF secretion by MIO-M1 cells upon
576 IL-6 treatment. High glucose concentrations of 25 mM potentiated the induction of VEGF by IL-6
577 (94). However, by default the standard culture medium used in our study has a D-glucose
578 concentration of 25 mM. Thus, an adaption of MIO-M1 cells to these conditions might have occurred
579 negating the induction of VEGF by IL-6.

580 Elevated levels of IFNγ in the vitreous of DR patients have been described previously (95, 96). In our
581 study, we could observe distinctly elevated INFγ secretion only after stimulation with INFγ.
582 Treatment with IFNγ furthermore induced the secretion of CXCL9, CXCL10, IL-6 and complement
583 subcomponent C1R in MIO-M1 cells and pRMG.

584 Interestingly, we observed an induction of CX3CL1 in the whole-cell lysates and in the secretomes.
585 Specifically, except for TGFβ1 and TGFβ2, all stimulants used in this study induced expression of
586 CX3CL1 in the cell proteome of MIO-M1 cells, while only IFNγ and TNFα treatment resulted in
587 significantly higher abundance of CX3CL1 in the secretome as well. CX3CL1 is a membrane-bound
588 chemokine, which functions as an adhesion molecule for leukocytes, but can also be proteolytically
589 cleaved, resulting in a soluble form with chemotactic function (97, 98). Several studies already
590 demonstrated the implication of CX3CL1 in DR pathogenesis as the vitreous of PDR patients
591 contains elevated levels of CX3CL1 (99) Furthermore, circulating CD11b+ leukocytes that are
592 involved in leukostasis in DR express higher levels of CX3CR1 in diabetic mice compared to
593 controls (100). Thus, membrane-bound CX3CL1 on the surface of Müller cells might be involved in
594 leukostasis in DR. Since TNFα levels are elevated in the eyes of DR patients, this might result in the
595 upregulation of CX3CL1 in diabetic Müller cells (101). In a previous study, incubation of microglia
596 with Müller cell supernatant containing secreted CX3CL1 resulted in the upregulation of the
597 respective receptor CX3CR1 in microglia. The authors proposed that Müller cells might be able to
598 promote microglial motility via the chemotactic effect of CX3CL1 (102). Thus, secretion of CX3CL1
599 from Müller cells might contribute to DR pathogenesis by recruiting peripheral inflammatory cells
600 and microglia. Upregulation of CX3CL1 after treatment with TNFα has been demonstrated in aortic
601 endothelial cells, but could not be observed in retinal endothelial cells (103). Here, we demonstrate
602 that stimulation with TNFα elicits secretion of CX3CL1 in pRMG and MIO-M1 cells and expression
603 of CX3CL1 in MIO-M1 cells. Thus, we lay the ground for further research concerning the expression
604 and regulation of CX3CL1 in Müller cells during DR.

605 Another route of communication between microglia/macrophages and Müller cells could be local
606 changes in complement expression. We recently demonstrated, that Müller cells in the mouse retina
607 are the main producers of complement components of the classical (C1s, C4), the alternative pathway
608 (FB) and C3 as the central component to all pathways under homeostatic, but also under ischemic
609 stress conditions (104). In the retina, it is the microglia that by far express highest levels of

610 complement receptors including ITGAM (alias CD11b), C3aR, C5aR1 and C5aR2 (104). In our
611 present study, TNFα and INFγ triggerd the most prominent effects on complement expression
612 consistently in MIO-M1 and pRMG. Given that *in vivo* microglia and potentially other immune cell
613 serve as major source of TNFα and INFγ (105) (resource data from Cowan et al., 2020 (106) at
614 https://data.iob.ch), the strong effect of these cytokines on Müller cell could be central to coordinate
615 the tissue immune homeostasis in pathologies. In this context, the enhanced expression of activating
616 complement components by Müller glia could serve as feedback mechanisms towards microglia in
617 turn modulating their activation profile. Taken together, our results point towards a pro-inflammatory
618 phenotype of Müller cells, which is in line with a previous study, where we analyzed the surfaceome
619 of primary equine Müller cells and MIO-M1 cells after stimulation with Lipopolysaccharide (30).
620 While the surfaceome of Müller cells in this previous study revealed expression of MHC class I and
621 II as well as costimulatory molecules especially in primary equine Müller cells, we could now further
622 complement these results with LC-MS/MS-analyses of whole cell lysates and of cell supernatants,
623 confirming an antigen-presenting phenotype of Müller cells. While stimulation with LPS resulted in
624 enhanced expression of MHC class II molecules in primary equine Müller cells, no MHC class II
625 molecules could be identified in MIO-M1 cells upon LPS treatment (30). In contrast, stimulation
626 with IFNγ in this study induced the expression of proteins that are associated with both MHC-I and
627 MHC-II antigen presentation in pRMG as well as in MIO-M1 cells. This is in accordance with an
628 early study that demonstrated the induction of MHC class I and MHC class II molecules in primary
629 human Müller cells by IFNγ *in vitro* (107). In contrast to MIO-M1 cells, pRMG also showed basal
630 expression of MHC class II without stimulation. Thus, our data demonstrate that Müller cells exhibit
631 several criteria for atypical antigen-presenting cells (108). While microglial cells are the predominant
632 immune cells of the retina, our data confirm that Müller cells are crucially involved in immunological
633 processes in the retina as well, as they possess an antigen processing and presenting machinery and
634 secrete pro-inflammatory cytokines (14). We have previously shown that the cultivation of primary
635 porcine Müller cells under hyperglycemic conditions resulted in higher expression levels of MHC
636 class II molecules, pointing towards an immunologically activated state of Müller cells in DR (36).

637 Besides expression of MHC class I and II molecules, we demonstrated that stimulation of Müller
638 cells with various cytokines resulted in the enrichment of proteins and pathways that are associated
639 with the formation and maturation of phagosomes. Previously, Müller cells have been described to be
640 phagocytic cells, capable of phagocytosing cell debris, dead photoreceptor cells and even bacteria
641 (109-111). Our IPA showed that proteins of phagocytosis pathways in Müller cells are induced upon
642 stimulation with various cytokines. Furthermore, phagocytosis is not only clathrin- but also caveolar-
643 mediated. Since our data showed enrichment of phagocytic pathways, as well as the canonical
644 antigen presentation pathway, it is possible that Müller cells present exogenous peptides on MHC
645 class II to CD4+ T helper cells. Intriguingly, phagocytosis of dead photoreceptors would also allow
646 Müller cells to present proteins expressed by photoreceptors on MHC class II, and via cross-
647 presentation on MHC class I (112, 113). The relationship of HLA alleles and haplotypes to the
648 progression of diabetic retinopathy is part of an ongoing scientific debate (114-122). However, the
649 rigorous pro-inflammatory signaling of Müller cells paired to potential activation of CD4+ and CD8+
650 T cells in the context of DR should be elaborated in further studies. Towards this goal it should be
651 addressed, whether Müller cells are sufficient to stimulate alloreactive naïve T cells or memory T
652 cells (108).

653 Furthermore, our proteomic analysis revealed significantly higher abundance of the costimulatory
654 molecule CD40 in pRMG after stimulation with IFNγ. Intriguingly, CD40 has been shown to play a
655 vital role in DR pathogenesis (123-125). A study with transgenic mice, which express CD40 only in
656 Müller cells, demonstrated that the upregulation of CD40 in Müller cells under diabetic conditions is

This is a provisional file, not the final typeset article

657 sufficient for thriving leukostasis and degeneration of capillaries, thus promoting retinal
658 inflammation and neurodegeneration in streptozotocin induced DR (124). Expression of CD40 has
659 also been demonstrated in primary human Müller cells and its ligation with CD154 resulted in
660 increased expression of ICAM-1 in Müller cells (123). Furthermore, it was shown that activation of
661 Müller cells through CD40 leads to an enhanced production of TNFα and IL-1β in bystander
662 microglia (124). Since several studies revealed an association between elevated levels of IFNγ and
663 DR, and stimulation of CNS astrocytes led to expression of CD40, IFNγ in DR might lead to the
664 upregulation of CD40 in Müller cells and thus promote chronic inflammation (126-129). Here, we
665 provide new insight in CD40 signaling in Müller cells, as IFNγ increased the expression of CD40,
666 whereas TGFβ2, TGFβ3, TNFα and VEGF resulted in lower abundance of CD40 in pRMG. Future
667 studies are needed to further investigate this issue, as the CD40 signaling pathway constitutes a
668 possibility for therapeutical intervention (130). In contrast to the porcine dataset, we could not
669 identify CD40 in the MIO-M1 cells. As CD40 expression has already been shown in primary human
670 Müller cells, our result might be due to the dedifferentiation of immortalized cells in culture (123).

671 Oxidative stress and reactive oxygen species (ROS) are known to play a central role during the
672 pathogenesis of DR (131). Rat-derived Müller cells under hyperglycemic conditions developed
673 mitochondrial dysfunction and oxidative stress, causing swelling and eventually apoptosis of the cells
674 (132, 133). Mitochondrial dysfunction can lead to ROS production, which then promotes
675 inflammatory response by activation of NF-κB and release of pro-inflammatory cytokines (134, 135).
676 Our analysis revealed that proteins associated with mitochondrial dysfunction were enriched after
677 treatment of pRMG with all tested cytokines. Furthermore, two significantly enriched pathways in
678 our data sets are associated with reactive oxygen species, namely "NRF2 mediated Oxidative Stress
679 Response" and "Production of Nitric Oxide and Reactive Oxygen Species in Macrophages".
680 Intriguingly, Müller cells have previously been found to regulate the ROS levels via Nrf2 and to be
681 more resistant to ROS formation compared to photoreceptor cells or bipolar cells (41, 136). In line
682 with this, we showed that treatment with IL-4, TGFβ2, TGFβ3, TNFα and VEGF inhibited death
683 receptor signaling pRMG. Phagocytic cells often produce ROS to protect themselves from pathogens
684 (137). Furthermore, macrophages stabilize cytosolic Nrf2 to be more resistant against ROS (138).
685 Since Müller cells have been shown to by phagocytic, we propose that induction of ROS in these
686 cells also serves as a defense mechanism (109-111).

687 In this study, we used both primary porcine Müller cells and the spontaneously immortalized human
688 Müller cell line MIO-M1 that was established and described in the Moorfields Institute of
689 Ophthalmology 2002 (39). Although MIO-M1 cells largely retain the phenotypic and functional
690 characteristics of Müller cells *in vitro*, previous studies documented some characteristics of neuronal
691 stem cells and expression of postmitotic neuronal cell markers in MIO-M1 cells (39, 139, 140).
692 Furthermore, it has been shown that Müller cells tend to adapt to cell culture conditions by reduced
693 secretion of neurotrophic factors (141-143). Our analysis revealed many proteins commonly
694 regulated in pRMG and MIO-M1 cells, as well as pathways similarly enriched and regulated in both
695 cells. However, we also observed effects specific for either MIO-M1 cells or pRMG. Thus, for
696 example our IPA revealed that MIO-M1 cells decrease the activity of the significantly enriched
697 canonical pathway oxidative phosphorylation, while it is amongst the most induced pathways of
698 pRMG following treatment with the majority of tested cytokines. While these differences might
699 originate from different adaption of MIO-M1 cells and pRMG to the cell culture conditions or the
700 immortalization of MIO-M1 cells, it might as well be possible that they originate from differences in
701 human and porcine Müller cells. Further studies should elaborate similarities and differences between
702 freshly prepared primary human and porcine Müller cells.

Taken together, our in-depth proteomic profiling of MIO-M1 cells and pRMG revealed the capacity of Müller cells to react in a differentiated manner upon treatment with various growth factors and cytokines. Furthermore, we demonstrated a primarily pro-inflammatory phenotype of Müller cells, as they secreted a variety of pro-inflammatory cytokines, complement components and upregulated proteins associated with antigen processing and presentation, suggesting a function as atypical antigen-presenting cell in the course of retinal inflammation. Furthermore, we observed enrichment of proteins connected to mitochondrial dysfunction, as well as proteins related to the formation and maturation of phagosomes. Thus, Müller cells are capable of modulating immune responses in the retina, and may significantly contribute to chronic inflammation during DR.

5 Conflict of Interest

The authors declare that the research was conducted in the absence of any commercial or financial relationships that could be construed as a potential conflict of interest.

6 Author Contributions

Conceptualization, S.M.H. and C.A.D.; Formal analysis, S.M.H.; Funding acquisition, S.M.H. and C.A.D.; Investigation, A.S., L.L., C.A.D., and S.M.H.; Project administration, S.M.H.; Supervision, S.M.H.; Visualization, A.S.; Writing - original draft, A.S., L.L., A.G., and D.P.; Writing - review and editing, C.A.D. and S.M.H. All authors have read and agreed to the published version of the manuscript.

7 Funding

This work was funded by Deutsche Forschungsgemeinschaft in the SPP 2127, grant numbers DFG DE 719/7-1 to C.A.D., HA 6014/5-1 to S.M.H., GR 4403/5-1 to A.G. and PA 1844/3-1 to D.P.

8 Acknowledgments

The authors would like to thank Adrian Sandbiller for providing porcine eye samples as well as Juliane Merl-Pham for critical discussions.

9 Data Availability Statement

All data are contained within the article or in supplementary materials.

This is a provisional file, not the final typeset article

730 **10 References**

731 1. Duncan JL, Pierce EA, Laster AM, Daiger SP, Birch DG, Ash JD, et al. Inherited Retinal
732 Degenerations: Current Landscape and Knowledge Gaps. Transl Vis Sci Technol. 2018;7(4):6.

733 2. Wooff Y, Man SM, Aggio-Bruce R, Natoli R, Fernando N. IL-1 Family Members Mediate
734 Cell Death, Inflammation and Angiogenesis in Retinal Degenerative Diseases. Front Immunol.
735 2019;10:1618.

736 3. Olivares-González L, Velasco S, Campillo I, Rodrigo R. Retinal Inflammation, Cell Death
737 and Inherited Retinal Dystrophies. Int J Mol Sci. 2021;22(4).

738 4. Forrester JV, Kuffova L, Delibegovic M. The Role of Inflammation in Diabetic Retinopathy.
739 Front Immunol. 2020;11:583687.

740 5. Broadgate S, Yu J, Downes SM, Halford S. Unravelling the genetics of inherited retinal
741 dystrophies: Past, present and future. Prog Retin Eye Res. 2017;59:53-96.

742 6. Lechner J, O'Leary OE, Stitt AW. The pathology associated with diabetic retinopathy. Vision
743 Research. 2017;139:7-14.

744 7. Collaborators GBaVI. Causes of blindness and vision impairment in 2020 and trends over 30
745 years, and prevalence of avoidable blindness in relation to VISION 2020: the Right to Sight: an
746 analysis for the Global Burden of Disease Study. Lancet Glob Health. 2021;9(2):e144-e60.

747 8. Chen M, Obasanmi G, Armstrong D, Lavery NJ, Kissenpfennig A, Lois N, et al. STAT3
748 activation in circulating myeloid-derived cells contributes to retinal microvascular dysfunction in
749 diabetes. J Neuroinflammation. 2019;16(1):138.

750 9. Gerhardinger C, Costa MB, Coulombe MC, Toth I, Hoehn T, Grosu P. Expression of acute-
751 phase response proteins in retinal Müller cells in diabetes. Invest Ophthalmol Vis Sci.
752 2005;46(1):349-57.

753 10. Mizutani M, Gerhardinger C, Lorenzi M. Müller cell changes in human diabetic retinopathy.
754 Diabetes. 1998;47(3):445-9.

755 11. Zeng HY, Green WR, Tso MO. Microglial activation in human diabetic retinopathy. Arch
756 Ophthalmol. 2008;126(2):227-32.

757 12. Coughlin BA, Feenstra DJ, Mohr S. Müller cells and diabetic retinopathy. Vision Research.
758 2017;139:93-100.

759 13. Kinuthia UM, Wolf A, Langmann T. Microglia and Inflammatory Responses in Diabetic
760 Retinopathy. Front Immunol. 2020;11:564077.

761 14. Karlstetter M, Scholz R, Rutar M, Wong WT, Provis JM, Langmann T. Retinal microglia:
762 just bystander or target for therapy? Prog Retin Eye Res. 2015;45:30-57.

763 15. Di Pierdomenico J, Martínez-Vacas A, Hernández-Muñoz D, Gómez-Ramírez AM, Valiente-
764 Soriano FJ, Agudo-Barriuso M, et al. Coordinated Intervention of Microglial and Müller Cells in
765 Light-Induced Retinal Degeneration. Invest Ophthalmol Vis Sci. 2020;61(3):47.

766 16. Wang M, Ma W, Zhao L, Fariss RN, Wong WT. Adaptive Müller cell responses to microglial
767 activation mediate neuroprotection and coordinate inflammation in the retina. J Neuroinflammation.
768 2011;8:173.

769 17. Reichenbach A, Bringmann A. Glia of the human retina. Glia. 2020;68(4):768-96.

770 18. Newman E, Reichenbach A. The Müller cell: a functional element of the retina. Trends
771 Neurosci. 1996;19(8):307-12.

772 19. Bringmann A, Pannicke T, Grosche J, Francke M, Wiedemann P, Skatchkov SN, et al. Müller
773 cells in the healthy and diseased retina. Prog Retin Eye Res. 2006;25(4):397-424.

774 20. Bringmann A, Iandiev I, Pannicke T, Wurm A, Hollborn M, Wiedemann P, et al. Cellular
775 signaling and factors involved in Müller cell gliosis: Neuroprotective and detrimental effects. Prog
776 Retin Eye Res. 2009;28(6):423-51.

777 21. Ruzafa N, Pereiro X, Lepper MF, Hauck SM, Vecino E. A Proteomics Approach to Identify
778 Candidate Proteins Secreted by Müller Glia that Protect Ganglion Cells in the Retina.
779 PROTEOMICS. 2018;18(11):1700321.

780 22. von Toerne C, Menzler J, Ly A, Senninger N, Ueffing M, Hauck SM. Identification of a
781 Novel Neurotrophic Factor from Primary Retinal Müller Cells Using Stable Isotope Labeling by
782 Amino Acids in Cell Culture (SILAC). Mol Cell Proteomics. 2014;13(9):2371-81.

783 23. Hauck SM, Schoeffmann S, Amann B, Stangassinger M, Gerhards H, Ueffing M, et al.
784 Retinal Mueller glial cells trigger the hallmark inflammatory process in autoimmune uveitis. J
785 Proteome Res. 2007;6(6):2121-31.

786 24. Subirada PV, Paz MC, Ridano ME, Lorenc VE, Vaglienti MV, Barcelona PF, et al. A journey
787 into the retina: Müller glia commanding survival and death. European Journal of Neuroscience.
788 2018;47(12):1429-43.

789 25. Ghaseminejad F, Kaplan L, Pfaller AM, Hauck SM, Grosche A. The role of Müller cell
790 glucocorticoid signaling in diabetic retinopathy. Graefes Arch Clin Exp Ophthalmol.
791 2020;258(2):221-30.

792 26. Natoli R, Fernando N, Madigan M, Chu-Tan JA, Valter K, Provis J, et al. Microglia-derived
793 IL-1β promotes chemokine expression by Müller cells and RPE in focal retinal degeneration. Mol
794 Neurodegener. 2017;12(1):31.

795 27. Rutar M, Natoli R, Chia RX, Valter K, Provis JM. Chemokine-mediated inflammation in the
796 degenerating retina is coordinated by Müller cells, activated microglia, and retinal pigment
797 epithelium. J Neuroinflammation. 2015;12(1):8.

798 28. Roberge FG, Caspi RR, Nussenblatt RB. Glial retinal Müller cells produce IL-1 activity and
799 have a dual effect on autoimmune T helper lymphocytes. Antigen presentation manifested after
800 removal of suppressive activity. J Immunol. 1988;140(7):2193-6.

801 29. Lorenz L, Amann B, Hirmer S, Degroote RL, Hauck SM, Deeg CA. NEU1 is more abundant
802 in uveitic retina with concomitant desialylation of retinal cells. Glycobiology. 2021.

803 30. Lorenz L, Hirmer S, Schmalen A, Hauck SM, Deeg CA. Cell Surface Profiling of Retinal
804 Muller Glial Cells Reveals Association to Immune Pathways after LPS Stimulation. Cells.
805 2021;10(3).

806 31. Middleton S. Porcine ophthalmology. Vet Clin North Am Food Anim Pract. 2010;26(3):557-
807 72.

808 32. Kleinwort KJH, Amann B, Hauck SM, Hirmer S, Blutke A, Renner S, et al. Retinopathy with
809 central oedema in an INS (C94Y) transgenic pig model of long-term diabetes. Diabetologia.
810 2017;60(8):1541-9.

This is a provisional file, not the final typeset article

811 33. Renner S, Blutke A, Clauss S, Deeg CA, Kemter E, Merkus D, et al. Porcine models for
812 studying complications and organ crosstalk in diabetes mellitus. Cell and Tissue Research. 2020.

813 34. Konigsberg IR, Borie R, Walts AD, Cardwell J, Rojas M, Metzger F, et al. Molecular
814 Signatures of Idiopathic Pulmonary Fibrosis. Am J Respir Cell Mol Biol. 2021.

815 35. Weigand M, Hauck SM, Deeg CA, Degroote RL. Deviant proteome profile of equine
816 granulocytes associates to latent activation status in organ specific autoimmune disease. J
817 Proteomics. 2021;230:103989.

818 36. Sagmeister S, Merl-Pham J, Petrera A, Deeg CA, Hauck SM. High glucose treatment
819 promotes extracellular matrix proteome remodeling in Mller glial cells. PeerJ. 2021;9:e11316.

820 37. Eberhardt C, Amann B, Stangassinger M, Hauck SM, Deeg CA. Isolation, characterization
821 and establishment of an equine retinal glial cell line: a prerequisite to investigate the physiological
822 function of Muller cells in the retina. J Anim Physiol Anim Nutr (Berl). 2012;96(2):260-9.

823 38. Hauck SM, Suppmann S, Ueffing M. Proteomic profiling of primary retinal Muller glia cells
824 reveals a shift in expression patterns upon adaptation to in vitro conditions. Glia. 2003;44(3):251-63.

825 39. Limb GA, Salt TE, Munro PM, Moss SE, Khaw PT. In vitro characterization of a
826 spontaneously immortalized human Muller cell line (MIO-M1). Invest Ophthalmol Vis Sci.
827 2002;43(3):864-9.

828 40. Wisniewski JR, Zougman A, Nagaraj N, Mann M. Universal sample preparation method for
829 proteome analysis. Nat Methods. 2009;6(5):359-62.

830 41. Grosche A, Hauser A, Lepper MF, Mayo R, von Toerne C, Merl-Pham J, et al. The Proteome
831 of Native Adult Muller Glial Cells From Murine Retina. Mol Cell Proteomics. 2016;15(2):462-80.

832 42. Kall L, Canterbury JD, Weston J, Noble WS, MacCoss MJ. Semi-supervised learning for
833 peptide identification from shotgun proteomics datasets. Nat Methods. 2007;4(11):923-5.

834 43. Navarro P, Trevisan-Herraz M, Bonzon-Kulichenko E, Nunez E, Martinez-Acedo P, Perez-
835 Hernandez D, et al. General statistical framework for quantitative proteomics by stable isotope
836 labeling. J Proteome Res. 2014;13(3):1234-47.

837 44. Benjamini Y, Drai D, Elmer G, Kafkafi N, Golani I. Controlling the false discovery rate in
838 behavior genetics research. Behav Brain Res. 2001;125(1-2):279-84.

839 45. Kramer A, Green J, Pollard J, Jr., Tugendreich S. Causal analysis approaches in Ingenuity
840 Pathway Analysis. Bioinformatics. 2014;30(4):523-30.

841 46. Fisher RA. On the Interpretation of χ^2 from Contingency Tables, and the Calculation of P.
842 Journal of the Royal Statistical Society. 1922;85(1):87-94.

843 47. Eisen MB, Spellman PT, Brown PO, Botstein D. Cluster analysis and display of genome-
844 wide expression patterns. Proc Natl Acad Sci U S A. 1998;95(25):14863-8.

845 48. Saldanha AJ. Java Treeview--extensible visualization of microarray data. Bioinformatics.
846 2004;20(17):3246-8.

847 49. Lunney JK, Ho CS, Wysocki M, Smith DM. Molecular genetics of the swine major
848 histocompatibility complex, the SLA complex. Dev Comp Immunol. 2009;33(3):362-74.

849 50. Sigal LJ. Activation of CD8 T Lymphocytes during Viral Infections. Encyclopedia of
850 Immunobiology. 2016:286-90.

This is a provisional file, not the final typeset article

851 51. Hewitt EW. The MHC class I antigen presentation pathway: strategies for viral immune
852 evasion. Immunology. 2003;110(2):163-9.

853 52. Roche PA, Furuta K. The ins and outs of MHC class II-mediated antigen processing and
854 presentation. Nat Rev Immunol. 2015;15(4):203-16.

855 53. Lechner J, O'Leary OE, Stitt AW. The pathology associated with diabetic retinopathy. Vision
856 Res. 2017;139:7-14.

857 54. Zheng Y, He M, Congdon N. The worldwide epidemic of diabetic retinopathy. Indian J
858 Ophthalmol. 2012;60(5):428-31.

859 55. Ginhoux F, Greter M, Leboeuf M, Nandi S, See P, Gokhan S, et al. Fate mapping analysis
860 reveals that adult microglia derive from primitive macrophages. Science. 2010;330(6005):841-5.

861 56. Coughlin BA, Feenstra DJ, Mohr S. Muller cells and diabetic retinopathy. Vision Res.
862 2017;139:93-100.

863 57. Wang J, Xu X, Elliott MH, Zhu M, Le YZ. Muller cell-derived VEGF is essential for
864 diabetes-induced retinal inflammation and vascular leakage. Diabetes. 2010;59(9):2297-305.

865 58. Bai Y, Ma JX, Guo J, Wang J, Zhu M, Chen Y, et al. Muller cell-derived VEGF is a
866 significant contributor to retinal neovascularization. J Pathol. 2009;219(4):446-54.

867 59. Demircan N, Safran BG, Soylu M, Ozcan AA, Sizmaz S. Determination of vitreous
868 interleukin-1 (IL-1) and tumour necrosis factor (TNF) levels in proliferative diabetic retinopathy. Eye
869 (Lond). 2006;20(12):1366-9.

870 60. Kelly K, Wang JJ, Zhang SX. The unfolded protein response signaling and retinal Muller cell
871 metabolism. Neural Regen Res. 2018;13(11):1861-70.

872 61. Zhong Y, Li J, Chen Y, Wang JJ, Ratan R, Zhang SX. Activation of endoplasmic reticulum
873 stress by hyperglycemia is essential for Muller cell-derived inflammatory cytokine production in
874 diabetes. Diabetes. 2012;61(2):492-504.

875 62. Zhang SX, Wang JJ, Gao G, Shao C, Mott R, Ma JX. Pigment epithelium-derived factor
876 (PEDF) is an endogenous antiinflammatory factor. FASEB J. 2006;20(2):323-5.

877 63. He J, Wang H, Liu Y, Li W, Kim D, Huang H. Blockade of vascular endothelial growth
878 factor receptor 1 prevents inflammation and vascular leakage in diabetic retinopathy. J Ophthalmol.
879 2015;2015:605946.

880 64. Liu Y, Li L, Pan N, Gu J, Qiu Z, Cao G, et al. TNF-alpha released from retinal Muller cells
881 aggravates retinal pigment epithelium cell apoptosis by upregulating mitophagy during diabetic
882 retinopathy. Biochem Biophys Res Commun. 2021;561:143-50.

883 65. Gilbert RWD, Vickaryous MK, Viloria-Petit AM. Signalling by Transforming Growth Factor
884 Beta Isoforms in Wound Healing and Tissue Regeneration. J Dev Biol. 2016;4(2).

885 66. Yaswen L, Kulkarni AB, Fredrickson T, Mittleman B, Schiffman R, Payne S, et al.
886 Autoimmune manifestations in the transforming growth factor-beta 1 knockout mouse. Blood.
887 1996;87(4):1439-45.

888 67. Yamagami S, Yokoo S, Mimura T, Amano S. Effects of TGF-beta2 on immune response-
889 related gene expression profiles in the human corneal endothelium. Invest Ophthalmol Vis Sci.
890 2004;45(2):515-21.

This is a provisional file, not the final typeset article

891 68. Huang T, Schor SL, Hinck AP. Biological activity differences between TGF-beta1 and TGF-
892 beta3 correlate with differences in the rigidity and arrangement of their component monomers.
893 Biochemistry. 2014;53(36):5737-49.

894 69. Kulkarni AB, Huh CG, Becker D, Geiser A, Lyght M, Flanders KC, et al. Transforming
895 growth factor beta 1 null mutation in mice causes excessive inflammatory response and early death.
896 Proc Natl Acad Sci U S A. 1993;90(2):770-4.

897 70. Shull MM, Ormsby I, Kier AB, Pawlowski S, Diebold RJ, Yin M, et al. Targeted disruption
898 of the mouse transforming growth factor-beta 1 gene results in multifocal inflammatory disease.
899 Nature. 1992;359(6397):693-9.

900 71. Sanford LP, Ormsby I, Gittenberger-de Groot AC, Sariola H, Friedman R, Boivin GP, et al.
901 TGFbeta2 knockout mice have multiple developmental defects that are non-overlapping with other
902 TGFbeta knockout phenotypes. Development. 1997;124(13):2659-70.

903 72. Proetzel G, Pawlowski SA, Wiles MV, Yin M, Boivin GP, Howles PN, et al. Transforming
904 growth factor-beta 3 is required for secondary palate fusion. Nat Genet. 1995;11(4):409-14.

905 73. Yang LT, Kaartinen V. Tgfb1 expressed in the Tgfb3 locus partially rescues the cleft palate
906 phenotype of Tgfb3 null mutants. Dev Biol. 2007;312(1):384-95.

907 74. Hall BE, Wankhade UD, Konkel JE, Cherukuri K, Nagineni CN, Flanders KC, et al.
908 Transforming growth factor-beta3 (TGF-beta3) knock-in ameliorates inflammation due to TGF-beta1
909 deficiency while promoting glucose tolerance. J Biol Chem. 2013;288(44):32074-92.

910 75. Schultz-Cherry S, Lawler J, Murphy-Ullrich JE. The type 1 repeats of thrombospondin 1
911 activate latent transforming growth factor-beta. J Biol Chem. 1994;269(43):26783-8.

912 76. Schultz-Cherry S, Murphy-Ullrich JE. Thrombospondin causes activation of latent
913 transforming growth factor-beta secreted by endothelial cells by a novel mechanism. J Cell Biol.
914 1993;122(4):923-32.

915 77. Murphy-Ullrich JE, Downs JC. The Thrombospondin1-TGF-beta Pathway and Glaucoma. J
916 Ocul Pharmacol Ther. 2015;31(7):371-5.

917 78. Conedera FM, Quintela Pousa AM, Presby DM, Mercader N, Enzmann V, Tschopp M.
918 Diverse Signaling by TGFbeta Isoforms in Response to Focal Injury is Associated with Either
919 Retinal Regeneration or Reactive Gliosis. Cell Mol Neurobiol. 2021;41(1):43-62.

920 79. Kaminska B, Gozdz A, Zawadzka M, Ellert-Miklaszewska A, Lipko M. MAPK signal
921 transduction underlying brain inflammation and gliosis as therapeutic target. Anat Rec (Hoboken).
922 2009;292(12):1902-13.

923 80. Tripathi RC, Li J, Chan WF, Tripathi BJ. Aqueous humor in glaucomatous eyes contains an
924 increased level of TGF-beta 2. Exp Eye Res. 1994;59(6):723-7.

925 81. Fuchshofer R, Birke M, Welge-Lussen U, Kook D, Lutjen-Drecoll E. Transforming growth
926 factor-beta 2 modulated extracellular matrix component expression in cultured human optic nerve
927 head astrocytes. Invest Ophthalmol Vis Sci. 2005;46(2):568-78.

928 82. Fuchshofer R. The pathogenic role of transforming growth factor-beta2 in glaucomatous
929 damage to the optic nerve head. Exp Eye Res. 2011;93(2):165-9.

930 83. Fuchshofer R, Tamm ER. The role of TGF-beta in the pathogenesis of primary open-angle
931 glaucoma. Cell Tissue Res. 2012;347(1):279-90.

This is a provisional file, not the final typeset article

932 84. Zode GS, Sethi A, Brun-Zinkernagel AM, Chang IF, Clark AF, Wordinger RJ. Transforming
933 growth factor-beta2 increases extracellular matrix proteins in optic nerve head cells via activation of
934 the Smad signaling pathway. Mol Vis. 2011;17:1745-58.

935 85. Mohammad G, Kowluru RA. Matrix metalloproteinase-2 in the development of diabetic
936 retinopathy and mitochondrial dysfunction. Lab Invest. 2010;90(9):1365-72.

937 86. Tan W, Zou JL, Yoshida S, Jiang B, Zhou YD. Increased vitreal levels of interleukin-10 in
938 diabetic retinopathy: a Meta-analysis. Int J Ophthalmol. 2020;13(9):1477-83.

939 87. Dace DS, Khan AA, Kelly J, Apte RS. Interleukin-10 promotes pathological angiogenesis by
940 regulating macrophage response to hypoxia during development. PLoS One. 2008;3(10):e3381.

941 88. Luzina IG, Keegan AD, Heller NM, Rook GA, Shea-Donohue T, Atamas SP. Regulation of
942 inflammation by interleukin-4: a review of "alternatives". J Leukoc Biol. 2012;92(4):753-64.

943 89. Major J, Fletcher JE, Hamilton TA. IL-4 pretreatment selectively enhances cytokine and
944 chemokine production in lipopolysaccharide-stimulated mouse peritoneal macrophages. J Immunol.
945 2002;168(5):2456-63.

946 90. Gadani SP, Cronk JC, Norris GT, Kipnis J. IL-4 in the brain: a cytokine to remember. J
947 Immunol. 2012;189(9):4213-9.

948 91. Yoshida S, Sotozono C, Ikeda T, Kinoshita S. Interleukin-6 (IL-6) production by cytokine-
949 stimulated human Muller cells. Curr Eye Res. 2001;22(5):341-7.

950 92. Yao Y, Li R, Du J, Long L, Li X, Luo N. Interleukin-6 and Diabetic Retinopathy: A
951 Systematic Review and Meta-Analysis. Curr Eye Res. 2019;44(5):564-74.

952 93. Liu X, Ye F, Xiong H, Hu DN, Limb GA, Xie T, et al. IL-1beta induces IL-6 production in
953 retinal Muller cells predominantly through the activation of p38 MAPK/NF-kappaB signaling
954 pathway. Exp Cell Res. 2015;331(1):223-31.

955 94. Coughlin BA, Trombley BT, Mohr S. Interleukin-6 (IL-6) mediates protection against
956 glucose toxicity in human Muller cells via activation of VEGF-A signaling. Biochem Biophys Res
957 Commun. 2019;517(2):227-32.

958 95. Ucgun NI, Zeki-Fikret C, Yildirim Z. Inflammation and diabetic retinopathy. Mol Vis.
959 2020;26:718-21.

960 96. Wu H, Hwang DK, Song X, Tao Y. Association between Aqueous Cytokines and Diabetic
961 Retinopathy Stage. J Ophthalmol. 2017;2017:9402198.

962 97. Bazan JF, Bacon KB, Hardiman G, Wang W, Soo K, Rossi D, et al. A new class of
963 membrane-bound chemokine with a CX3C motif. Nature. 1997;385(6617):640-4.

964 98. Imai T, Hieshima K, Haskell C, Baba M, Nagira M, Nishimura M, et al. Identification and
965 molecular characterization of fractalkine receptor CX3CR1, which mediates both leukocyte
966 migration and adhesion. Cell. 1997;91(4):521-30.

967 99. Abu El-Asrar AM, Nawaz MI, Ahmad A, De Zutter A, Siddiquei MM, Blanter M, et al.
968 Evaluation of Proteoforms of the Transmembrane Chemokines CXCL16 and CX3CL1, Their
969 Receptors, and Their Processing Metalloproteinases ADAM10 and ADAM17 in Proliferative
970 Diabetic Retinopathy. Front Immunol. 2020;11:601639.

971 100. Serra AM, Waddell J, Manivannan A, Xu H, Cotter M, Forrester JV. CD11b+ bone marrow-
972 derived monocytes are the major leukocyte subset responsible for retinal capillary leukostasis in

This is a provisional file, not the final typeset article

973 experimental diabetes in mouse and express high levels of CCR5 in the circulation. Am J Pathol.
974 2012;181(2):719-27.

975 101. Wu F, Phone A, Lamy R, Ma D, Laotaweerungsawat S, Chen Y, et al. Correlation of
976 Aqueous, Vitreous, and Plasma Cytokine Levels in Patients With Proliferative Diabetic Retinopathy.
977 Invest Ophthalmol Vis Sci. 2020;61(2):26.

978 102. Zhang S, Zhang S, Gong W, Zhu G, Wang S, Wang Y, et al. Muller Cell Regulated
979 Microglial Activation and Migration in Rats With N-Methyl-N-Nitrosourea-Induced Retinal
980 Degeneration. Front Neurosci. 2018;12:890.

981 103. Greene JA, Portillo JA, Lopez Corcino Y, Subauste CS. CD40-TRAF Signaling Upregulates
982 CX3CL1 and TNF-alpha in Human Aortic Endothelial Cells but Not in Retinal Endothelial Cells.
983 PLoS One. 2015;10(12):e0144133.

984 104. Pauly D, Agarwal D, Dana N, Schafer N, Biber J, Wunderlich KA, et al. Cell-Type-Specific
985 Complement Expression in the Healthy and Diseased Retina. Cell Rep. 2019;29(9):2835-48 e4.

986 105. Kaczmarek-Hajek K, Zhang J, Kopp R, Grosche A, Rissiek B, Saul A, et al. Re-evaluation of
987 neuronal P2X7 expression using novel mouse models and a P2X7-specific nanobody. Elife. 2018;7.

988 106. Cowan CS, Renner M, De Gennaro M, Gross-Scherf B, Goldblum D, Hou Y, et al. Cell
989 Types of the Human Retina and Its Organoids at Single-Cell Resolution. Cell. 2020;182(6):1623-40
990 e34.

991 107. Mano T, Tokuda N, Puro DG. Interferon-gamma induces the expression of major
992 histocompatibility antigens by human retinal glial cells. Exp Eye Res. 1991;53(5):603-7.

993 108. Kambayashi T, Laufer TM. Atypical MHC class II-expressing antigen-presenting cells: can
994 anything replace a dendritic cell? Nat Rev Immunol. 2014;14(11):719-30.

995 109. Bejarano-Escobar R, Sanchez-Calderon H, Otero-Arenas J, Martin-Partido G, Francisco-
996 Morcillo J. Muller glia and phagocytosis of cell debris in retinal tissue. J Anat. 2017;231(4):471-83.

997 110. Sakami S, Imanishi Y, Palczewski K. Muller glia phagocytose dead photoreceptor cells in a
998 mouse model of retinal degenerative disease. FASEB J. 2019;33(3):3680-92.

999 111. Singh PK, Shiha MJ, Kumar A. Antibacterial responses of retinal Muller glia: production of
1000 antimicrobial peptides, oxidative burst and phagocytosis. J Neuroinflammation. 2014;11:33.

1001 112. Gutierrez-Martinez E, Planes R, Anselmi G, Reynolds M, Menezes S, Adiko AC, et al. Cross-
1002 Presentation of Cell-Associated Antigens by MHC Class I in Dendritic Cell Subsets. Front Immunol.
1003 2015;6:363.

1004 113. Larsson M, Fonteneau JF, Bhardwaj N. Dendritic cells resurrect antigens from dead cells.
1005 Trends Immunol. 2001;22(3):141-8.

1006 114. Kastelan S, Tomic M, Salopek-Rabatic J, Pavan J, Lukenda A, Gotovac M, et al. The
1007 association between the HLA system and retinopathy development in patients with type 1 diabetes
1008 mellitus. Coll Antropol. 2013;37 Suppl 1:65-70.

1009 115. Barbosa J, Ramsay RC, Knobloch WH, Cantrill HL, Noreen H, King R, et al.
1010 Histocompatibility antigen frequencies in diabetic retinopathy. Am J Ophthalmol. 1980;90(2):148-
1011 53.

1012 116. Dornan TL, Ting A, McPherson CK, Peckar CO, Mann JI, Turner RC, et al. Genetic
1013 susceptibility to the development of retinopathy in insulin-dependent diabetics. Diabetes.
1014 1982;31(3):226-31.

1015 117. Falck AA, Knip JM, Ilonen JS, Laatikainen LT. Genetic markers in early diabetic retinopathy
1016 of adolescents with type I diabetes. J Diabetes Complications. 1997;11(4):203-7.

1017 118. Cruickshanks KJ, Vadheim CM, Moss SE, Roth MP, Riley WJ, Maclaren NK, et al. Genetic
1018 marker associations with proliferative retinopathy in persons diagnosed with diabetes before 30 yr of
1019 age. Diabetes. 1992;41(7):879-85.

1020 119. Birinci A, Birinci H, Abidinoglu R, Durupinar B, Oge I. Diabetic retinopathy and HLA
1021 antigens in type 2 diabetes mellitus. Eur J Ophthalmol. 2002;12(2):89-93.

1022 120. Agardh D, Gaur LK, Agardh E, Landin-Olsson M, Agardh CD, Lernmark A. HLA-
1023 DQB1*0201/0302 is associated with severe retinopathy in patients with IDDM. Diabetologia.
1024 1996;39(11):1313-7.

1025 121. Santos DC, Porto LC, Pizarro MH, de Melo LGN, Silva DA, Oliveira RV, et al. Human
1026 Leukocyte Antigens class II (HLA II) gene profile from an admixed population of patients with type
1027 1 diabetes with severe diabetic retinopathy: a nested case-control study in Brazil. Diabetol Metab
1028 Syndr. 2021;13(1):83.

1029 122. Liu C, Chen G, Bentley AR, Doumatey A, Zhou J, Adeyemo A, et al. Genome-wide
1030 association study for proliferative diabetic retinopathy in Africans. NPJ Genom Med. 2019;4:20.

1031 123. Portillo JA, Greene JA, Okenka G, Miao Y, Sheibani N, Kern TS, et al. CD40 promotes the
1032 development of early diabetic retinopathy in mice. Diabetologia. 2014;57(10):2222-31.

1033 124. Portillo JC, Lopez Corcino Y, Miao Y, Tang J, Sheibani N, Kern TS, et al. CD40 in Retinal
1034 Müller Cells Induces P2X7-Dependent Cytokine Expression in Macrophages/Microglia in Diabetic
1035 Mice and Development of Early Experimental Diabetic Retinopathy. Diabetes. 2017;66(2):483-93.

1036 125. Subauste CS. The CD40-ATP-P2X 7 Receptor Pathway: Cell to Cell Cross-Talk to Promote
1037 Inflammation and Programmed Cell Death of Endothelial Cells. Front Immunol. 2019;10:2958.

1038 126. Cvitkovic K, Sesar A, Sesar I, Pusic-Sesar A, Pejic R, Kelava T, et al. Concentrations of
1039 Selected Cytokines and Vascular Endothelial Growth Factor in Aqueous Humor and Serum of
1040 Diabetic Patients. Semin Ophthalmol. 2020;35(2):126-33.

1041 127. Ozay Y, Ozek D, Yildirim F, Yildirim Z. The effect of diabetes on vitreous levels of
1042 adiponectin and inflammatory cytokines in experimental rat model. Adv Clin Exp Med.
1043 2020;29(4):449-52.

1044 128. Vujosevic S, Micera A, Bini S, Berton M, Esposito G, Midena E. Proteome analysis of retinal
1045 glia cells-related inflammatory cytokines in the aqueous humour of diabetic patients. Acta
1046 Ophthalmol. 2016;94(1):56-64.

1047 129. Tan L, Gordon KB, Mueller JP, Matis LA, Miller SD. Presentation of proteolipid protein
1048 epitopes and B7-1-dependent activation of encephalitogenic T cells by IFN-gamma-activated SJL/J
1049 astrocytes. J Immunol. 1998;160(9):4271-9.

1050 130. Portillo JC, Yu JS, Hansen S, Kern TS, Subauste MC, Subauste CS. A cell-penetrating CD40-
1051 TRAF2,3 blocking peptide diminishes inflammation and neuronal loss after ischemia/reperfusion.
1052 FASEB J. 2021;35(3):e21412.

1053 131. Cecilia OM, Jose Alberto CG, Jose NP, Ernesto German CM, Ana Karen LC, Luis Miguel
1054 RP, et al. Oxidative Stress as the Main Target in Diabetic Retinopathy Pathophysiology. J Diabetes
1055 Res. 2019;2019:8562408.

This is a provisional file, not the final typeset article

1056 132. Tien T, Zhang J, Muto T, Kim D, Sarthy VP, Roy S. High Glucose Induces Mitochondrial
1057 Dysfunction in Retinal Muller Cells: Implications for Diabetic Retinopathy. Invest Ophthalmol Vis
1058 Sci. 2017;58(7):2915-21.

1059 133. Krugel K, Wurm A, Pannicke T, Hollborn M, Karl A, Wiedemann P, et al. Involvement of
1060 oxidative stress and mitochondrial dysfunction in the osmotic swelling of retinal glial cells from
1061 diabetic rats. Exp Eye Res. 2011;92(1):87-93.

1062 134. Behl T, Kotwani A. Exploring the various aspects of the pathological role of vascular
1063 endothelial growth factor (VEGF) in diabetic retinopathy. Pharmacol Res. 2015;99:137-48.

1064 135. Homme RP, Singh M, Majumder A, George AK, Nair K, Sandhu HS, et al. Remodeling of
1065 Retinal Architecture in Diabetic Retinopathy: Disruption of Ocular Physiology and Visual Functions
1066 by Inflammatory Gene Products and Pyroptosis. Front Physiol. 2018;9:1268.

1067 136. Wang J, Shanmugam A, Markand S, Zorrilla E, Ganapathy V, Smith SB. Sigma 1 receptor
1068 regulates the oxidative stress response in primary retinal Muller glial cells via NRF2 signaling and
1069 system xc(-), the Na(+)-independent glutamate-cystine exchanger. Free Radic Biol Med. 2015;86:25-
1070 36.

1071 137. Geng J, Sun X, Wang P, Zhang S, Wang X, Wu H, et al. Kinases Mst1 and Mst2 positively
1072 regulate phagocytic induction of reactive oxygen species and bactericidal activity. Nat Immunol.
1073 2015;16(11):1142-52.

1074 138. Wang P, Geng J, Gao J, Zhao H, Li J, Shi Y, et al. Macrophage achieves self-protection
1075 against oxidative stress-induced ageing through the Mst-Nrf2 axis. Nat Commun. 2019;10(1):755.

1076 139. Hollborn M, Ulbricht E, Rillich K, Dukic-Stefanovic S, Wurm A, Wagner L, et al. The
1077 human Muller cell line MIO-M1 expresses opsins. Mol Vis. 2011;17:2738-50.

1078 140. Lawrence JM, Singhal S, Bhatia B, Keegan DJ, Reh TA, Luthert PJ, et al. MIO-M1 cells and
1079 similar muller glial cell lines derived from adult human retina exhibit neural stem cell characteristics.
1080 Stem Cells. 2007;25(8):2033-43.

1081 141. Merl J, Ueffing M, Hauck SM, von Toerne C. Direct comparison of MS-based label-free and
1082 SILAC quantitative proteome profiling strategies in primary retinal Muller cells. Proteomics.
1083 2012;12(12):1902-11.

1084 142. Hauck SM, Gloeckner CJ, Harley ME, Schoeffmann S, Boldt K, Ekstrom PA, et al.
1085 Identification of paracrine neuroprotective candidate proteins by a functional assay-driven
1086 proteomics approach. Mol Cell Proteomics. 2008;7(7):1349-61.

1087 143. von Toerne C, Menzler J, Ly A, Senninger N, Ueffing M, Hauck SM. Identification of a
1088 novel neurotrophic factor from primary retinal Muller cells using stable isotope labeling by amino
1089 acids in cell culture (SILAC). Mol Cell Proteomics. 2014;13(9):2371-81.

1090